frontiers in Ecology and Evolution

ORIGINAL RESEARCH
published: 15 December 2020
doi: 10.3389/fevo.2020.567109

Trends in Stable Isotopes and Climate Proxies From Late Changhsingian Ghost Landscapes of the Karoo Basin, South Africa

Robert A. Gastaldo[1], Neil J. Tabor[2] and Johann Neveling[3]*

[1] Department of Geology, Colby College, Waterville, ME, United States, [2] Department of Earth Science, Southern Methodist University, Dallas, TX, United States, [3] Council for Geoscience, Pretoria, South Africa

The stable carbon- and oxygen-isotope values derived from *in situ* pedogenic carbonate-cemented nodules and vertebrate apatite in the *Daptocephalus* and overlying *Lystrosaurus* Assemblage Zones of the Balfour Formation, Karoo Basin, South Africa, have formed the basis for previous interpretations of a unidirectional climate trend toward hyper-aridity across the biozone boundary. This assemblage-zone boundary has been considered by many authors to be equivalent to the Permian–Triassic boundary in the basin. To better understand the climate under which these vertebrate assemblages existed, we have analyzed the carbon- and oxygen-stable isotopes of pedogenic carbonate nodules sampled from fourteen horizons of intraformational pedogenic nodular conglomerate (PNC) at Old Lootsberg Pass, a classic locality at which the Permian–Triassic boundary is reported. Analysis of these refractory soil constituents provides insight into the climate under which these "ghost" soils formed, where no other physical record of their existence is found in the stratigraphy. A positive correlation between $\delta^{13}C_{VPDB}$ and $\delta^{18}O_{VSMOW}$ values of micrite cements is defined by analyses of carbonate nodules taken from a measured stratigraphic thickness of ∼200 m, which spans the biozone boundary as currently defined. For samples taken from the same lag deposit, similar and relatively narrow ranges of isotope values are encountered. Samples cluster into two isotopic groups. The values in the first group cluster more tightly in all sampled nodules ($\delta^{13}C_{VPDB}$ −2.3 to −6.5‰; $\delta^{18}O_{VSMOW}$ 13.8–15.1‰), and are interpreted to indicate that these originated from paleosols that formed under similar climate controls. Values from the second sample group display a wider variance between analyses ($\delta^{13}C_{VPDB}$ −5.2 to 14.0‰; $\delta^{18}O_{VSMOW}$ 8.8–15.5‰). These nodules are interpreted to indicate that they originated under polygenetic soil-forming conditions representing the reworking of either: (1) more than one paleosol, the calcite-cemented nodules of which represent precipitation under both closed and open-system controls; or (2) one or more compound-composite paleosols. Stable-isotope trends based on PNCs analyzed, thus far, demonstrate an overall shift over time in the ghost landscapes. More seasonally dry soils formed under a climate that can be characterized as warm/dry accompanied by lower precipitation in the lower part of the section. In contrast, soils in

OPEN ACCESS

Edited by:
Martin Daniel Ezcurra, Museo Argentino de Ciencias Naturales Bernardino Rivadavia, Argentina

Reviewed by:
Léa Leuzinger, University of Buenos Aires, Argentina
Pia Alexa Viglietti, Field Museum of Natural History, United States

****Correspondence:***
Robert A. Gastaldo
ragastal@colby.edu

Specialty section:
This article was submitted to Paleontology, a section of the journal Frontiers in Ecology and Evolution

Received: *29 May 2020*
Accepted: *12 November 2020*
Published: *15 December 2020*

Citation:
Gastaldo RA, Tabor NJ and Neveling J (2020) Trends in Stable Isotopes and Climate Proxies From Late Changhsingian Ghost Landscapes of the Karoo Basin, South Africa. Front. Ecol. Evol. 8:567109. doi: 10.3389/fevo.2020.567109

the upper part of the section formed under cool and moist conditions, with increased precipitation near the biozone boundary. Hence, latest Permian climate associated with the more seasonally dry landscapes demonstrate a trend toward cooler and wetter conditions, which is opposite to the trend widely held in the literature.

Keywords: end permian, *Daptocephalus* assemblage zone, *Lystrosaurus* assemblage zone, carbon isotopes, oxygen isotopes

INTRODUCTION

The paleontological, sedimentological, and geochemical records preserved in the Balfour Formation, Beaufort Group, Karoo Supergroup, South Africa (**Figure 1**), have long played a pivotal role in our reconstruction of the biological trends and physical factors responsible for how terrestrial ecosystems responded to the end-Permian crisis. Several authors interpret a stepwise turnover of vertebrate faunas in response to vegetational loss (Ward et al., 2005; Smith and Botha-Brink, 2014; Botha et al., 2020) followed by a rapid faunal recovery (Botha and Smith, 2006) in a Late Permian landscape affected by increased temperatures and aridity (but see Li et al., 2017; Gastaldo et al., 2019, 2020b). Two phases of vertebrate turnover, reported from an ∼30 m interval and interpreted by these authors as representing a mass extinction (but see Lucas, 2017, 2018), are reported in the *Daptocephalus* Assemblage Zone (AZ; Smith and Botha-Brink, 2014; Botha et al., 2020; Viglietti, 2020). The third extinction phase and faunal recovery are reported to occur in the overlying *Lystrosaurus* AZ (Viglietti et al., 2017), and the boundary between the two assemblage zones is considered by many as the terrestrial expression of the Permian–Triassic boundary (Benton and Newell, 2014; Bernardi et al., 2018). This interpretation, though, has been revised by Gastaldo et al. (2020a) who report an U-Pb CA-ID-TIMS latest Permian age (252.24 ± 0.11 Ma, 2 σ) on a pristine airfall ash horizon in the lower part of the *Lystrosaurus declivis* AZ (Botha and Smith, 2020). Nevertheless, the interpretation of a unidirectional paleoclimate trend across this interval is based, in large part, on the stable carbon- and oxygen-isotope records conserved in vertebrate tusks and large, *in situ* carbonate-cemented nodules (MacLeod et al., 2000, 2017; Rey et al., 2016). These samples originate from lithologies placed into coarse and generalized stratigraphies from various parts of the basin, correlated on the recognition of a "unique" event bed (Smith and Ward, 2001; Smith and Botha-Brink, 2014; Botha et al., 2020), thought to represent "continuous" sedimentation across the latest Permian and earliest Triassic (e.g., Smith, 1995; Botha et al., 2020). This latter assumption of a "continuous" sedimentary record is problematic with the recognition that the rocks of the Balfour Group mainly represent aggradational sediment packages punctuated by episodes of landscape degradation (Pace et al., 2009; Gastaldo and Demko, 2011; Gastaldo et al., 2018). Residual elements of these eroded landscapes–calcite-cemented pedogenic nodules (**Figure 1**), soil peds, vertebrate bone, and euhedral pyrite–are found as fluvial channel-lag deposits above erosional unconformities, which are distributed unpredictably through the stratigraphy of the Balfour and Katberg formations. Analyses of the carbon- and oxygen-stable isotopic composition of these reworked pedogenic carbonate nodules (PNC) provide insight into the prevailing latest Permian soil-forming environments and the climate(s) under which they formed. These findings offer important insights to a "missing" part of the geological record in the Karoo Basin, what we term "ghost" landscapes, because there is little physical record of their existence as *in situ* calcareous soil profiles. Hence, using these PNC stratigraphic units as proxy evidence for paleosol profiles, we offer new insights for the latest Permian reconstruction of environmental and climatic trends of those missing stratigraphic intervals in a high resolution stratigraphic framework in the Eastern Cape Province to test the hypothesis of unidirectional warming across the *Daptocephalus–Lystrosaurus declivis* Assemblage Zones.

GENERAL GEOLOGIC CONTEXT

The Karoo Basin formed ahead of the rising Cape Fold Belt (Lindeque et al., 2011; Viglietti et al., 2017), with initial sediments derived from continental deglaciation in the Late Carboniferous (Johnson et al., 2006). This succession, known as the Karoo Supergroup, comprises the basal Dwyka (Upper Carboniferous) and Ecca (Lower–Middle Permian) groups, the Beaufort (Middle Permian–Middle Triassic) and Stormberg (informal unit; Upper Triassic–Lower Jurassic; Catuneanu et al., 2005) groups, and culminates in the basaltic lavas of the Drakensberg Group (Lower Jurassic). Glacially-transported and glacial outwash sediments dominate marine turbidite successions of the Dwyka and Ecca groups, whereas the overlying Beaufort Group is fully continental in origin and shows no sign of any marine influence. The Beaufort Group is subdivided into the lower Adelaide and upper Tarkastad subgroups, of which the Balfour Formation in the former has been assigned to the Upper Permian to Lower Triassic and Katberg Formation, in the latter, to the Lower Triassic by the South South African Committee for Stratigraphy [SACS] (1980) and Johnson et al. (2006) (**Figure 1**). Traditionally, the Beaufort Group formation-and-member subdivision is based on the relative proportion of coarse- and fine-grained deposits, the number of sandstone packages, and predominant siltstone color in the area where the unit was described and codified.

Continental deposits represent a broad spectrum of both fluvial (coarse) and fluvial and interfluvial (fine) floodplain environments. Fluvial deposits range from fine- to very fine-grained sandstone of varying architectural elements and hierarchies, and range in color from yellowish gray to light-to-medium gray. These deposits commonly are exposed along

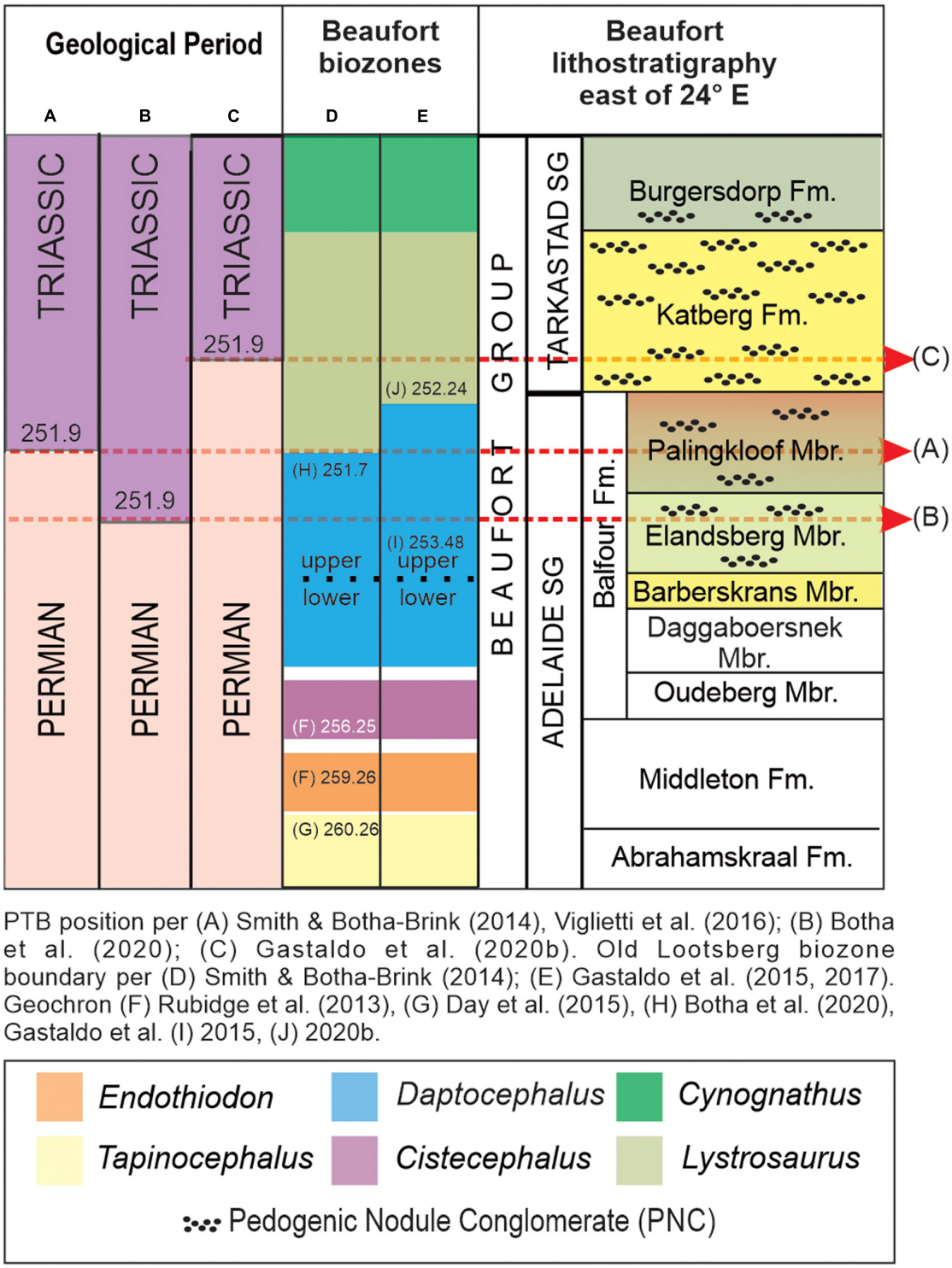

FIGURE 1 | General litho- and vertebrate biostratigraphy of the Upper Permian and Lower Triassic succession, Karoo Basin, South Africa, with constraining geochronometric age assignments. The boundary between the *Daptocephalus* and *Lystrosaurus* Assemblage Zones is interpreted by several workers **(A)** as equivalent with the end-Permian event (dashed red line) in the oceans. Recently, an Early Triassic detrital zircon age has been published for the *Daptocephalus* AZ **(B)**, implying that the biozone boundary has to be moved into the Mesozoic. In contrast, geochronometric constraints published for the *Daptocephalus* and *Lystrosaurus* AZs from ashfall deposits **(C)** restrict both to the latest Permian, demonstrating that the biozone boundary is not coincident with the marine extinction event. All workers place this boundary in the uppermost Balfour Formation, although Gastaldo et al. (2015, 2017, 2018) place the boundary higher **(E)** at Old Lootsberg Pass than **(D)** Smith and Botha-Brink (2014). We follow the scheme of Gastaldo et al. (2018, 2020a). The distribution of intraformational pedogenic nodule conglomerate ranges from the Elandberg Member to the Burgersdorp Formation. All dates are in Ma.

major roadways and railways, and act as the resistant caprock of many escarpments. In contrast, intraformational conglomerate is very uncommon and, in general, restricted to lenticular channel-lag deposits above erosional unconformities at the base of some channel bodies. Isolated lenticular beds of intraformational conglomerate also may occur in siltstone. The coloration of mudchip-conglomerate lags reflects the fine-grained clastic rip-up clasts found, therein, which range from variants of olive-gray or reddish-gray mudstone, or are a reddish brown when comprised of calcite-cemented nodules and other features of pedogenic origin. In-channel fluvial deposits may be of a heterolithic character, whereas overbank deposits of fine clastics include coarse and fine greenish-gray or reddish-gray mudrock, in which paleosols, early diagenetic pedogenic features, and trace fossils may be preserved (Smith, 1995; Retallack et al., 2003; Tabor et al., 2007; Gastaldo and Rolerson, 2008; Gastaldo et al., 2014, 2020b). Although heterolithic playa deposits are reported in the Balfour Formation in which their reddish coloration is attributable to eolian dust input (Smith and Botha-Brink, 2014), there is no physical, chemical, or regionally correlative evidence in support of this depositional environment or its interpretation (Gastaldo et al., 2019). Deposits resulting from volcaniclastic input originating from the Cape Fold Belt activity are rare but, when present, are represented by silicified porcellanite beds (Gastaldo et al., 2015, 2018), kaolinized tuff (Gastaldo et al., 2020a), and reworked tuffaceous siltstone (Gastaldo et al., 2018) from which geochronometric constraints are possible. But, prior to either data from which a magnetostratigraphy (De Kock and Kirschvink, 2004; Gastaldo et al., 2018) or chronostratigraphy (Rubidge et al., 2013; Gastaldo et al., 2015, 2020a) could be developed, the relatively monotonous nature of Beaufort Group rocks, and difficulties in both circumscribing lithostratigraphic units and their correlation across the basin, led early workers to subdivide these rocks using fossil-vertebrate assemblages (**Figure 1**). This vertebrate paradigm, in turn, was used to circumscribe uppermost Permian from lowermost Triassic deposits (Rubidge, 1995; Neveling et al., 2016a,b; Gastaldo et al., 2019).

Broom (1906) was the first to assign specimens of *Lystrosaurus* to the Triassic and placed the underlying biozones, including the interval now encompassing the *Daptocephalus* AZ (Viglietti et al., 2016), into the Late Permian. His sixfold biozonation (Broom, 1911) was revised by Kitching (1971, 1977), with subsequent modifications by Keyser and Smith (1978) and Keyser (1979), and were accepted by the South African Committee for Stratigraphy as formal nomenclature (South African Committee for Stratigraphy [SACS], 1980). Subsequently, this nomenclature was expanded (Rubidge, 1995) to an eightfold biozonation system and, again, refined during a recent review (Smith et al., 2020). Gastaldo et al. (2017, 2018, 2019, 2020a) have questioned the continued recognition of discrete *Daptocephalus* and *Lystrosaurus* (= *L. declivis* AZ; Viglietti, 2020) biozones in the basin, applying the vertebrate database of Smith and Botha-Brink (2014) in both the Eastern Cape Province and the Free State localities. The first U-Pb ID-TIMS ages for the lower part of the Adelaide Subgroup were published by Rubidge et al. (2013) (**Figure 1D**) and supplemented by an age estimate of 260.26 ± 0.081 Ma from a tuff near the top of the underlying *Tapinocephalus* AZ (Day et al., 2015). The first high resolution U-Pb CA-ID-TIMS ages on zircons from two horizons in the uppermost exposures of the Adelaide Subgroup were reported from the *Daptocephalus* AZ in the upper part of the Balfour Formation. Both horizons are placed in a tightly constrained litho- and magnetostratigraphic framework at Old Lootsberg Pass (Gastaldo et al., 2015, 2018). The horizon interpreted as a synsedimentary silicified ash (= porcellanite; Gastaldo et al., 2015, 2018) in the Elandsberg Member has yielded an early Changhsingian age (253.48 ± 0.15 Ma; Gastaldo et al., 2015). The second horizon is a well-silicified siltstone-trough fill, either in the uppermost Elandsberg Member or in the lowermost Palingkloof Member, and yields a detrital zircon population of Wuchiapingian age (256.8 ± 0.6 Ma; Gastaldo et al., 2018). This second age estimate is of a reworked deposit from an older ashfall deposit in response to landscape degradation (Gastaldo and Demko, 2011) and redeposition into a younger landform. Recently, an early Triassic age of 251.7 ± 0.3 Ma has been assigned to the upper *Daptocephalus* AZ by Botha et al. (2020) (**Figure 1B**) based on a detrital zircon population recovered from a sandstone below the *Daptocephalus/Lystrosaurus declivis* assemblage boundary on farm Nooitgedacht in the Free State Province. These authors equate the position of that sample to one below their vertebrate-defined End Permian Mass Extinction horizon. This age assignment contrasts dramatically with that of a latest Permian age U-Pb CA-ID-TIMS zircon age of 252.24 ± 0.11 (2σ) Ma from a thin, pristine air-fall deposit in magnetostratigraphic, palynostratigraphic, and geochemical context for the base of the *Lystrosaurus declivis* AZ from the same locality (Gastaldo et al., 2020a; **Figure 1C**). We have retained the geochronologic context of the vertebrate biostratigraphy presented by Gastaldo et al. (2020a) in the current study (**Figure 1C**). While these findings indicate that the *Daptocephalus/Lystrosaurus declivis* assemblage boundary, as currently defined, should be decoupled from the end-Permian extinction record in the marine record, the question remains as to whether a faunal turnover is associated with this biozone boundary or if it is associated with any climatic change that may have had global significance.

LOCALITY, MATERIALS, AND METHODS

The Eastern Cape Province hosts several classic localities reported to contain the transition from the *Daptocephalus* AZ to the *Lystrosaurus declivis* AZ, several of which are within a few kilometers of each other (**Figure 2**). These include Old Lootsberg Pass (= West Lootsberg Pass; Ward et al., 2000, 2005; Smith and Botha-Brink, 2014), Tweefontein (Smith and Botha-Brink, 2014), and Lootsberg Pass (= East Lootsberg Pass; Ward et al., 2000, 2005; Smith and Botha-Brink, 2014). Gastaldo et al. (2017, 2018) have noted that GPS coordinates reported by previous workers for published composite stratigraphic sections in these localities are inaccurate and unreliable (**Figure 2**). Hence, we have undertaken the development of a stratigraphic framework

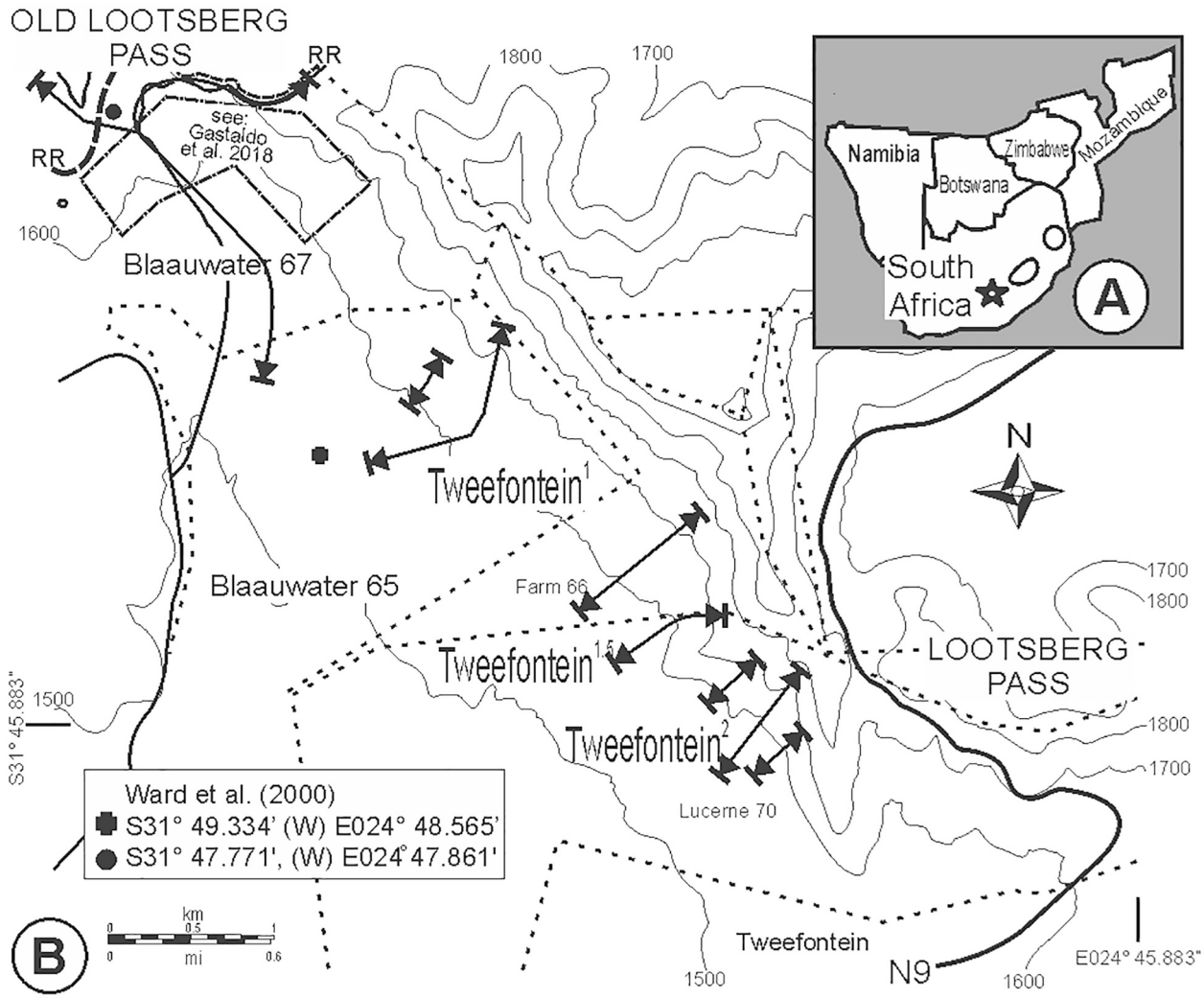

FIGURE 2 | Locality maps for the current study. **(A)** Generalized geographic map of southern Africa highlighting the study site in the Eastern Cape Province with a star. **(B)** Five localities in the Eastern Cape Province–Old (West) Lootsberg Pass, Tweefontein[1] (Gastaldo et al., 2017), Tweefontein[1.5] (reported here), Tweefontein[2] (refers to the section measured in an erosional gully closest to the vertebrate fossil assigned to Tweefontein by Smith and Botha-Brink, 2014), and Lootsberg Pass–reported as foundational to the terrestrial, end-Permian extinction model (Ward et al., 2000, 2005; Smith and Botha-Brink, 2014). Eight of the eleven measured stratigraphic sections used in the current study to develop a stratigraphic framework for the area are represented by solid black lines with arrows marking the base and top. GPS coordinates for the base and top of each are provided in **Figure 4**. Dotted lines mark former farm boundaries with names as they appear on with the 3124DD Lootsberg 1:50,000 map which, currently, are owned by Justin and Liesl Kingwill, Blaauwater Farm. Published GPS coordinates for Old (West) Lootsberg Pass (solid circle) and Tweefontein (solid polygon) sections (Ward et al., 2000), corrected for longitude, are plotted. The published Tweefontein fossil localities (Smith and Botha-Brink, 2014) are > 3 km to the southeast of the published GPS coordinates, and appears here as Tweefontein[2]. Scale in km and mi; contour interval 100 m.

beginning at Old Lootsberg Pass southeastward along the escarpment toward Lootsberg Pass that, now, consists of twenty-two measured sections totaling more than 1,500 m of section. Stratigraphic sections were measured using a leveling Jacob staff and Abney level, following procedures presented elsewhere (e.g., Gastaldo et al., 2017; Li et al., 2017), and lithologic field descriptions follow our previously published studies (Gastaldo et al., 2014, 2018). Stratigraphic sections have been physically correlated by walking and waypointing (GPS coordinates taken every 40–80 m) the upper contacts (bounding surfaces) of major fluvial complexes which provide for true datums in the area. We have traced individual sandstone bounding surfaces over a > 4 km lateral distance (**Figure 3**). We have estimated that intraformational pedogenic nodule conglomerate (PNC), relative to other lithofacies, accounts for less than 0.1% of rock volume in this area (Gastaldo et al., 2018). There is no predictive model as to where this lithofacies may occur. When encountered and logistically feasible, hand or drill-core samples of intraformational conglomerates were obtained for carbon and oxygen stable-isotope analyses (**Figures 3**, **4**) and paleomagnetic studies (Gastaldo et al., 2018). Five PNC samples originate in the western half of the study area (Old Lootsberg Pass,

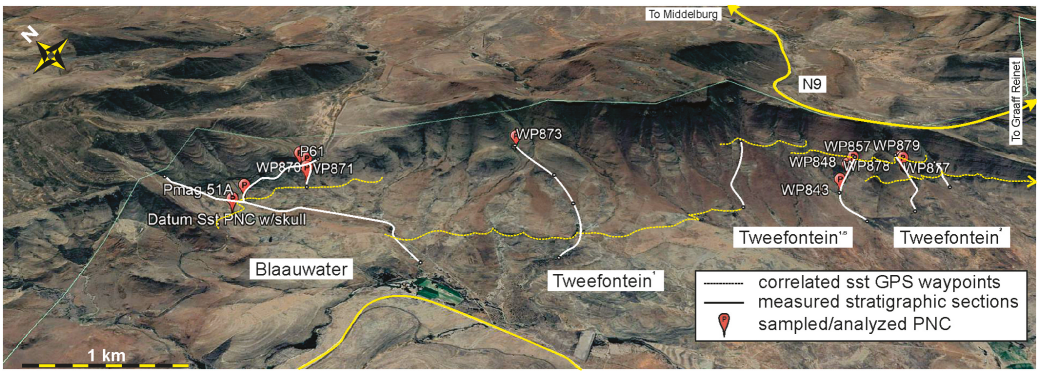

FIGURE 3 | Six of the measured sections at Old Lootsberg Pass to Tweefontein[2] (white solid lines; **Figure 2**) plotted on an oblique GoogleEarth image showing their spatial relationship relative to topography. Yellow dotted lines are laterally traceable sandstone-channel deposits, waypointed and used as datums for correlation across the area (**Figure 4**). Sampled intraformational pedogenic nodule conglomerates (PNC), identified with their waypoint (WP) designation, appear as red balloons. Scale = 1 km.

Tweefontein[1]); nine samples originate in the eastern half of the study area (Tweefontein[1.5], Tweefontein[2]).

Stable-Isotope Geochemistry

Micrite-cemented nodules from PNC deposits were cut at Southern Methodist University (SMU), described, and analyzed for carbon- and oxygen-stable isotopes following Gastaldo et al. (2014). Micrite- and microspar-cement samples were drilled from nodules using an x, y, z drill mount. Sample powders, varying from 2 to 10 mg for each carbonate-extraction experiment, were reacted with 100% orthophosphoric acid at 25°C *in vacuo*, under closed-system conditions to produce CO_2 (McCrea, 1950). CO_2 gas was cryogenically purified, measured for yields of CO_2 using a mercury manometer, and analyzed for stable carbon- and oxygen-isotope compositions using an Finigan MAT 252 isotope-ratio mass spectrometer housed in the Department of Earth Sciences at SMU. Yields of CO_2 resulting from each experiment were used to calculate wt.% $CaCO_3$ values for each sample based on the assumption that 1 mol of CO_2 represents the mass of 1 mol of $CaCO_3$. As is standard practice with interpretations of stable-isotope geochemistry of pedogenic carbonates, no sample with less than 50 wt.% $CaCO_3$ was further considered (e.g., Ekart et al., 1999; Sheldon and Tabor, 2009). However, it is noteworthy that no sample analyzed in this study contained < 50 wt.% $CaCO_3$.

Stable-isotope measurements are reported in standard delta notation in units of per mil (‰):

$$\delta^{13}C \text{ (or } \delta^{18}O) = (R_{sample}/R_{standard} - 1)^{*}1000, \quad (1)$$

where R = $^{13}C/^{12}C$ and $^{18}O/^{16}O$ for carbon and oxygen, respectively. $\delta^{13}C$ values are reported with respect to the Vienna Pee Dee Belemnite standard (VPDB; Craig, 1957); $\delta^{18}O$ is reported with respect to both the Vienna Pee Dee Belemnite standard (VPDB) and Vienna Standard Mean Ocean Water (VSMOW; Gonfiantini, 1984).

Multiple analyses were undertaken on all samples (**Supplementary Table 1**). Although within-nodule isotopic variability is observed to different degrees in rock powders from the basin, that variability is likely an intrinsic characteristic of an individual nodule. This reflects that, in conjunction with CO_2 samples extracted from powders of the Karoo basin rocks, an internal carbonate standard composed of Carrara marble was included as a separate analysis within each "batch" of analyses (typically 5—11 unknowns for each standard). The running mean (n = 17) of this Carrara marble standard over the period of analysis for this project is −2.34 ± 0.05‰ for $\delta^{13}C_{VPDB}$ values and −5.90 ± 0.10‰ for $\delta^{18}O_{VSMOW}$ values. Therefore, variability of within-sample stable carbon- and oxygen-isotope delta values of greater than 0.1 and 0.2‰, respectively, may be regarded as analytically different. Due to the fact that the number of samples analyzed per PNC deposit are small, which precludes the determination as to whether the data set consists of normally distributed values, neither parametric nor non-parametric statistical tests were undertaken.

RESULTS

Pedogenic Nodule Conglomerate Lithofacies

The PNC lithofacies is a matrix-supported intraformational pebble-conglomerate comprised of small (< 0.5–5 cm diameter) calcite-cemented nodules, rip-up mudclasts, and bone fragments in a very fine-grained wacke and/or coarse siltstone (**Figure 5**). Unweathered rock is pale olive (10 Y 6/2) but weathers on the surface to a range of colors including moderate yellowish brown (10 YR 5/4), dusky brown (5 YR 2/2), or brownish black (5 YR 2/1). Both nodules and matrix are calcite cemented.

Sandstone benches in which PNC conglomerate lags occur can be traced over a distance of several kilometers, depending on orientation and exposure (**Figure 4**). PNC accumulations range in geometries from thin (3—10 cm) to medium thick (0.1—0.3 m) lenses with undulatory bases that are in sharp erosional contact with underlying siltstone and/or sandstone. Thicker accumulations are organized into planar to lenticular crossbed sets of up to 1 m in thickness (**Figure 5**). Primary

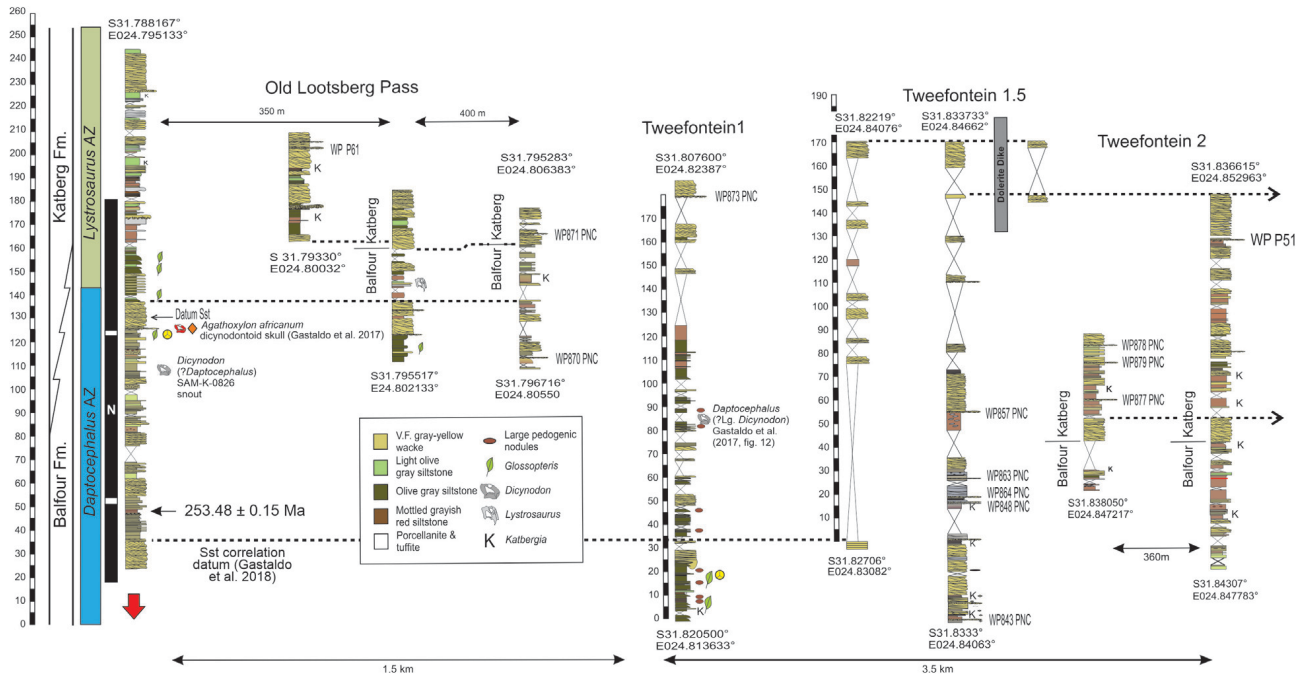

FIGURE 4 | Measured stratigraphic sections correlated using traceable sandstone-channel deposits (dotted lines) in which sampled intraformational pedogenic nodule conglomerate (PNC) are identified with their waypoint (WP) designation. Dotted lines of sandstone datums to the right in the diagram continue to the east around the nose of the escarpment to Lootsberg Pass (measured and correlated sections not shown). GPS coordinates of measured sections are provided, the U-Pb CA ID-TIMS age from a porcellanite as reported by Gastaldo et al. (2018) is placed in magnetostratigraphic context, and selected vertebrates of the *Daptocephalus* Assemblage Zone (blue vertical bar) noted in the Old Lootsberg Pass and Tweefontein[1] sections (see Gastaldo et al., 2017). The boundary between the *Daptocephalus* and *Lystrosaurus* (light green) AZs follows our previously published placement (Gastaldo et al., 2017, 2018). If the definition for the base of the Katberg Formation advanced by Johnson (1976) is applied to individual sections–the horizon above which there is a marked increase in sandstone abundance–this boundary plots at multiple horizons. Thus, the Balfour—Katberg formation boundary is shown as a transition zone (Johnson, 1976; Groenewald, 1996). Vertical scale in 5 m intervals.

sedimentary structures vary from planar to low-angle trough or sigmoidal cross beds (**Figure 5D**). Cobble-, pebble-, and sand-sized clasts are normal graded in all beds and mudchips may be up to 20 cm in length (**Figures 5**, **6**); grain shape is highly variable and includes subangular to subrounded morphologies of mudchips. Pedogenic nodule shape varies from sub-rounded rods to well-rounded ellipses and spheres, whereas other clasts appear amorphous (**Figure 6**).

Stable-Isotope Geochemistry

Diagenetic Considerations

A persistent issue with the interpretation of carbon- and oxygen-stable isotope values of ancient carbonates is screening, recognizing, and accommodating the effects of diagenesis. The problem is that the diagenetic alteration of pristine calcite in any nodule will be calcite; hence, there is no significant compositional/mineralogical difference to recognize one phase from the other. In studies of marine calcites, there is a broad array of minor-, rare-, and trace-element analyses which may be employed to evaluate some kinds of diagenetic alteration (e.g., Grossman et al., 1996). But, unfortunately, these do not apply to soil environments because of the extremely broad array of chemistries and redox conditions which may exist in soil-forming environments compared with shallow marine carbonate depositional systems. Nevertheless, numerous studies have articulated guidelines for screening diagenesis within soil-and-paleosol carbonates (e.g., Deutz et al., 2001; Sheldon and Tabor, 2009). Fundamentally, the best provisions that can be made to avoid values originated from diagenetic calcite are: (1) avoid sparry and coarsely crystalline phases, which are not typical (but not exclusive) of soil carbonates (e.g., Ekart et al., 1999) and; (2) choose samples with microcrystalline textures (micrite, microspar) that make up at least half of the mass of the paleosol nodule (Sheldon and Tabor, 2009). This minimum wt.% $CaCO_3$ is reported to ensure that the sample originally had an abundance of pedogenic calcite, and any additional material added by diagenetic alteration would be relatively small. We have employed these precautions in the current study and consider their application as the best efforts that can be taken to minimize the impacts of diagenesis.

$\delta^{13}C_{vpdb}$ Values of Pedogenic Nodules

Pedogenic nodule $\delta^{13}C_{VPDB}$ values of micrite cements range from −14.2 to −1.7‰ (−2.34 ± 0.05‰), with the sample suite of nodules from individual beds exhibiting either a tighter or wider spread of values (**Figure 7A** and **Table 1**). For example, the minimum and maximum values of six separate analyses of nodules from the WP- P51 PNC (**Figure 6E**) differ by

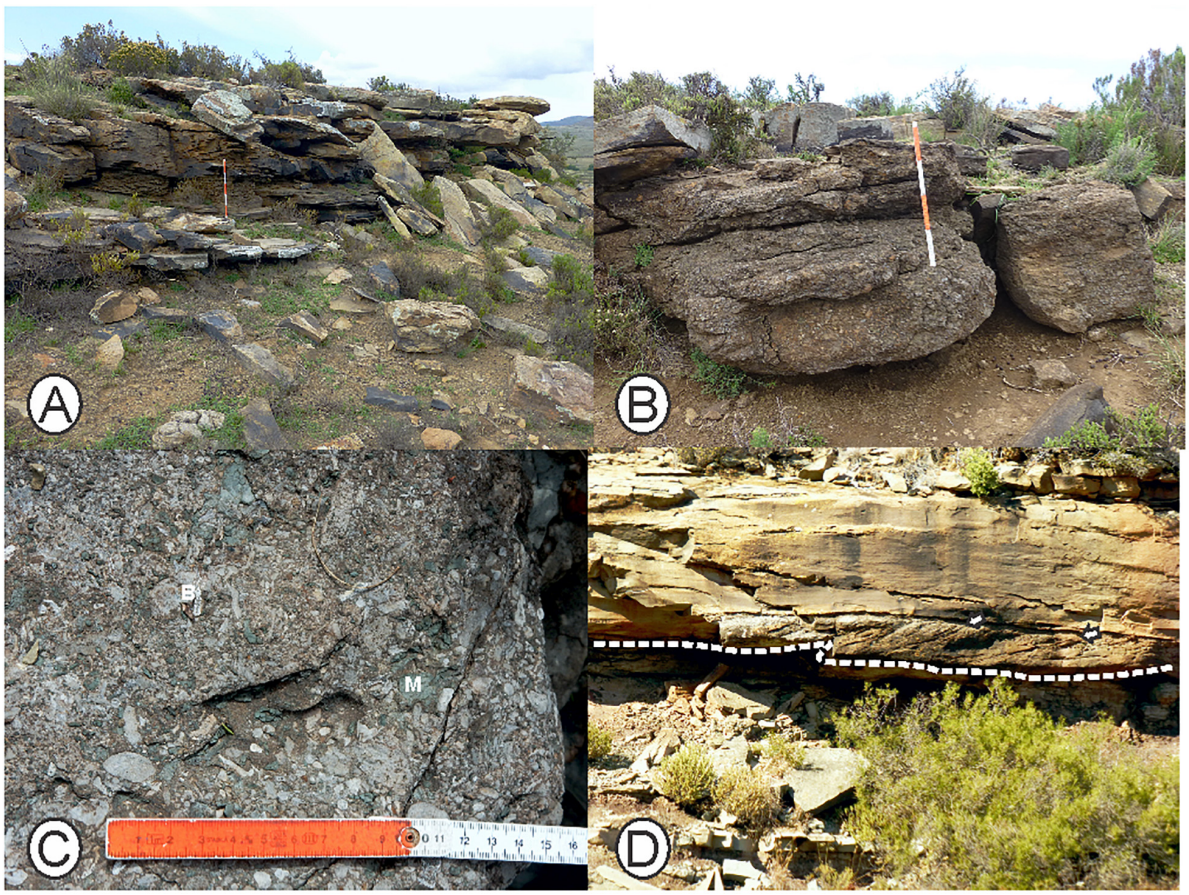

FIGURE 5 | Field images of intraformational PNC lag deposits. **(A)** 0.5 m thick lenticular deposit overlying an erosional base of the lowermost correlative sandstone in the area of Tweefontein[1] (**Figure 4**). Scale in dm and cm. **(B)** ∼1.0 m thick lenticular PNC in same area as **(A)** showing low angle crossbeds and surficial weathering coloration. Scale in dm. **(C)** Surface exposure of PNC in which greenish-gray mudchips (m) and vertebrate bone (b) are mixed with pedogenic nodules of various shapes and sizes. Scale in cm. **(D)** 1.0 m thick PNC lag exhibiting sigmoidal cross bedding. **(A–C)** S31.82372°, E024.81617°; **(D)** S31.76592°, E024.84473°.

1.0‰, and of four separate analyses of nodules from WP878 (**Figure 6D**), WP879, and WP848 PNCs exhibit a range of 1.1, 0.8, and 1.5‰, respectively. In contrast, the difference between the minimum and maximum values obtained for four separate analyses of nodules from sample WP857 (**Figure 6C**) and WP870 PNC units is 3.5, and 6.2‰, respectively, whereas values from two PNC horizons–P877 (N = 3) and WP864 (N = 3)–exceed 7.5‰ (**Table 1**). When PNC values are averaged per lag deposit, there is a discrete separation of collections with nine more positive and five more negative horizons (**Figure 7B**; PNC lags at WP857 and WP877, and WP870 and WP879, are considered to be separate horizons due to their spatial distribution and geochemical differences). Intervals of more positive values are interspersed with intervals of more negative values stratigraphically higher in the section.

$\delta^{18}O_{VSMOW}$ Values of Pedogenic Nodules

The $\delta^{18}O_{VSMOW}$ values obtained from micrite cements of the pedogenic nodule suite range from 8.7 to 16.9‰ (-5.90 ± 0.1‰), with individual conglomerate assemblages also exhibiting either a tight clustering or wider spread of values (**Figure 7C** and **Table 1**). For example, the minimum and maximum values for four separate analyses of nodules from the WP857 PNC, four separate analyses of nodules from the WP863 PNC (**Figures 4**, **7**), four separate analyses of nodules from the WP878 PNC, and six separate analyses of nodules from the P51 PNC differ by only 0.4, 1.2, 1.2, and 1.3‰, respectively. In contrast, the difference between the maximum and minimum values for nodules sampled at WP879 (N = 4), WP848 (N = 5), and WP864 (N = 4) is 3.2, 2.6, and 3.4‰, respectively. The $\delta^{18}O$ variance of pedogenic nodules in any sampled PNC bed mimics and complements that found in the $\delta^{13}C$ data set, either tightly clustering or exhibiting a wider spread. Unlike the distribution of values in the $\delta^{13}C$ data set, only two horizons–WP870 and Datum sst–stand out by having comparatively low $\delta^{18}O$ values (**Figure 7D**).

DISCUSSION

Carbonate crystallization in soils is related to a number of physical and chemical factors including temperature, evapotranspiration, soil acidity, and the availability of metal

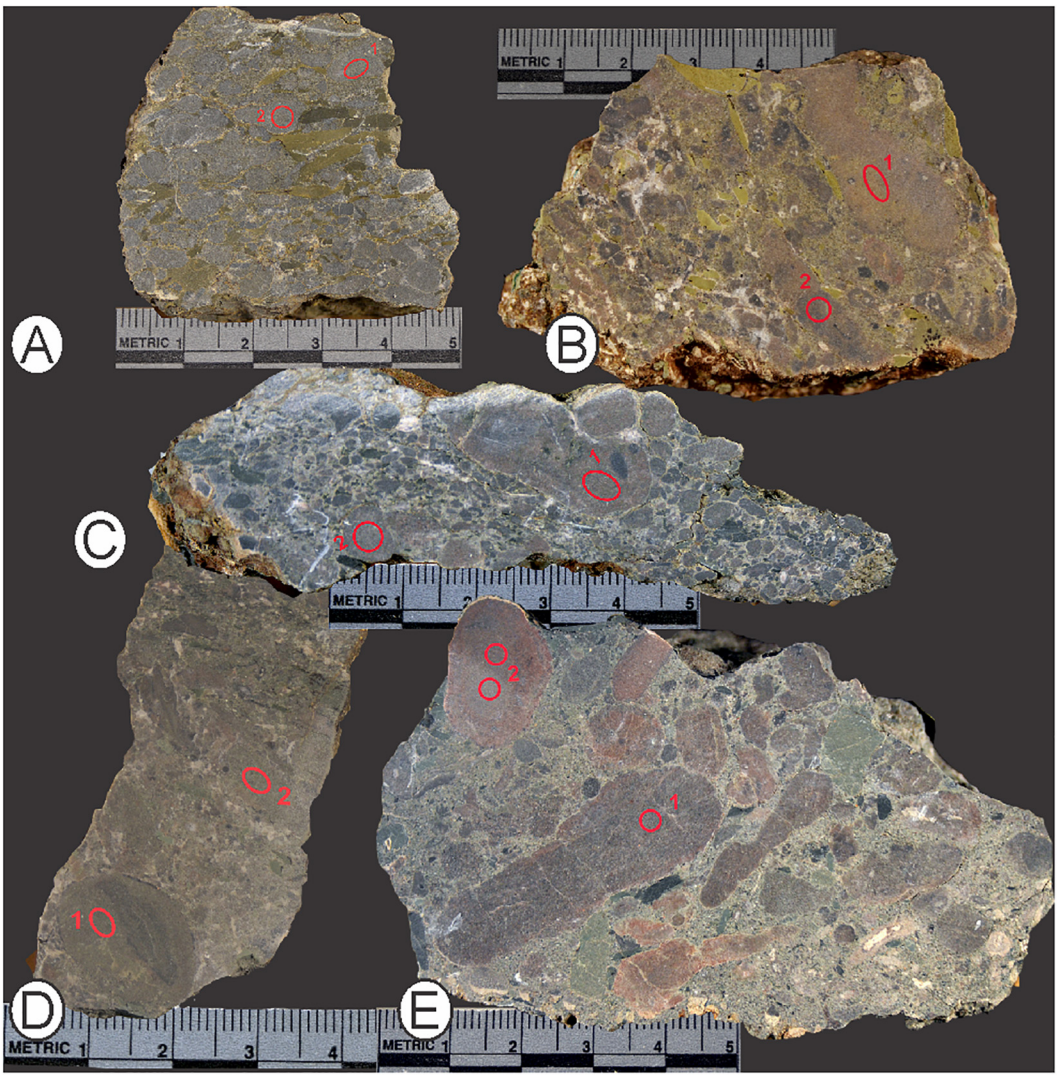

FIGURE 6 | Representative cut-and-sampled PNCs (see **Figure 4** for reference). **(A)** P61 recovered from the uppermost PNC bed at Old Lootsberg Pass. Drilled areas of two nodules are identified. **(B)** WP843 recovered from the base of Tweefontein$^{1.5}$ section with sample drill sites indicated. **(C)** WP857 recovered from the uppermost PNC in the Tweefontein$^{1.5}$ section; sampled nodules are identified. **(D)** WP878 recovered from the uppermost PNC lag in a short Tweefontein^{2} section where sampled nodules are identified. **(E)** P51 recovered from the uppermost PNC horizon at Tweefontein^{2}. Sites sampled for stable carbon- and oxygen-isotope values are indicated on two nodules. Scales in cm and mm.

cations (Ca^{+2}, Fe^{+2}, and Mg^{+2}; Sheldon and Tabor, 2009). As such, both $\delta^{13}C$ and $\delta^{18}O$ values derived from calcite cements of pedogenic nodules are widely used as paleoenvironmental proxies for the soil conditions under which these soil carbonates precipitated. Pedogenic stable-carbon isotope values include the carbon signal and contribution from bacterial decomposition of organic matter (Tabor et al., 2007) and that of atmospheric CO_2 in the local soil environment (see Sheldon and Tabor, 2009). In contrast, pedogenic $\delta^{18}O$ values derive from soil water which is related to meteoric waters, and is correlated (albeit very complicatedly) with mean annual temperature (MAT) and mean annual precipitation (MAP; Cerling, 1984; Cerling and Quade, 1993). In general, soil carbonates develop under seasonally wet-dry climates and rainfall < 850 mm/yr (Cerling, 1984; Royer, 1999), although pedogenic carbonate may precipitate in hydromorphic soils where groundwater fluctuates on a seasonal basis (e.g., Freytet and Plaziat, 1982; Slate et al., 1996).

A paradigm exists in Karoo Basin literature that considers carbonate precipitates found as pedogenic nodule cement as reflecting a contribution of CO_2 derived directly from the atmosphere (Ward et al., 2005; MacLeod et al., 2017; Botha et al., 2020). The stable isotopic signatures of these calcite cements are interpreted as having been in equilibrium with pCO_2 at the time of crystallization. This paradigm has been used to deduce Middle (Retallack et al., 2006) and Late Permian (MacLeod et al., 2000, 2017) climate trends using $\delta^{13}C_{VPDB}$ values obtained from *in situ* (dm-scale) pedogenic nodules placed in composite and very generalized stratigraphic order.

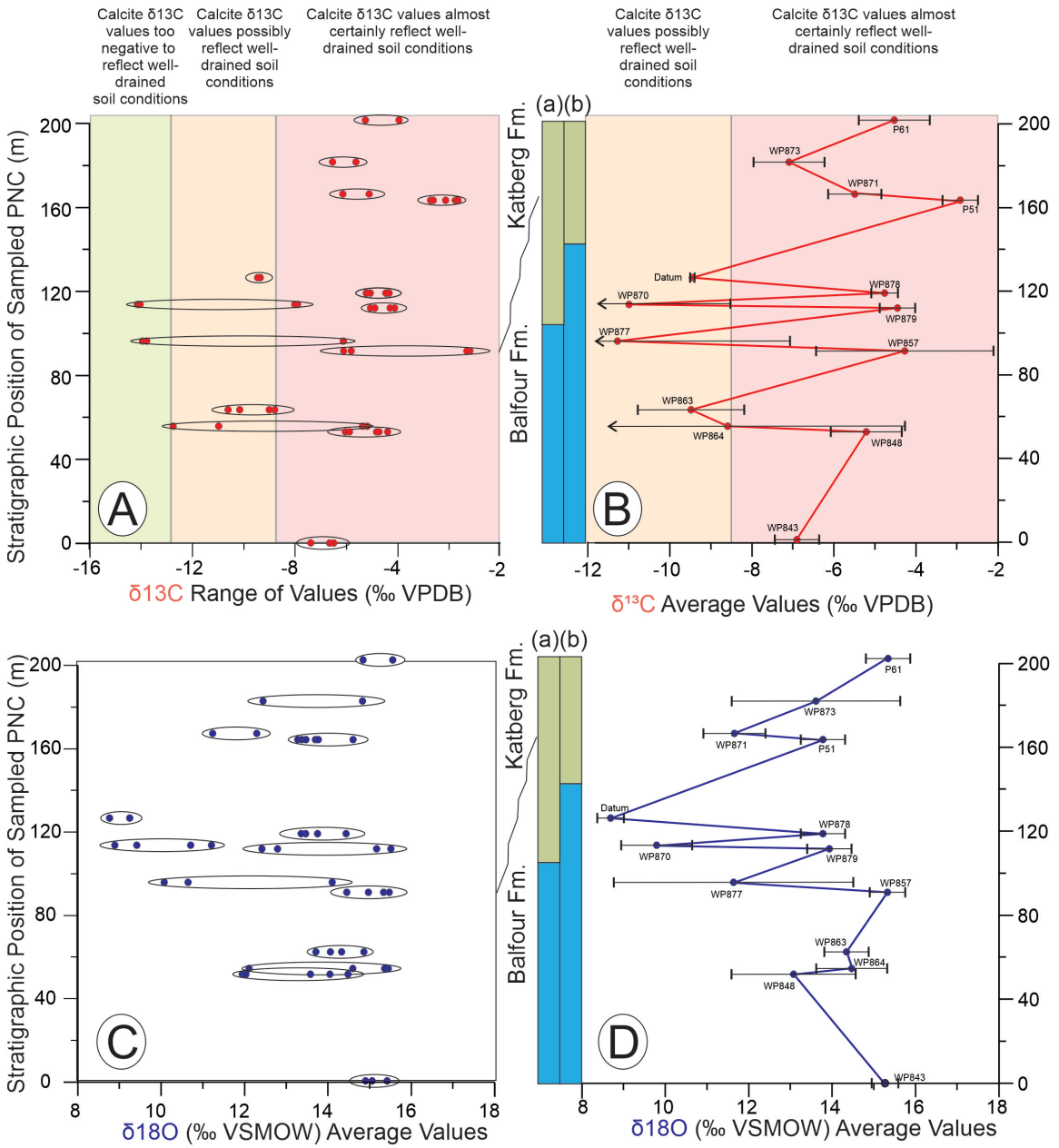

FIGURE 7 | Plots of $\delta^{13}C_{VPDB}$ and $\delta^{18}O_{VSMOW}$ values in stratigraphic order through the upper *Daptocephalus* (blue bar) and lower *Lystrosaurus* (light green bar) Assemblage Zones. Placement of the biozone boundary follows Smith and Botha-Brink (2014) on the left; on the right, placement follows Gastaldo et al. (2017, 2018). **(A)** Plot showing variation in $\delta^{13}C$ values for each sampled horizon against interpreted paleosol conditions under which calcite cement precipitated. **(B)** Plot of mean $\delta^{13}C_{VPDB}$ value for each sampled horizon against interpreted paleosol conditions under which calcite cement precipitated. **(C)** Plot showing variation in $\delta^{18}O_{VSMOW}$ values for each sampled horizon. **(D)** Plot of mean $\delta^{18}O_{VSMOW}$ value for each sampled horizon against sampled position in the *Daptocephalus* and *Lystrosaurus* Assemblage Zones. Standard deviation is provided around the mean values. Note that bimodal data exhibit a larger standard deviation.

Tabor et al. (2007) demonstrated that the variation of $\delta^{13}C_{VPDB}$ values of unaltered micrite and microspar cements in pedogenic nodules are a function of the weighted mean contribution of the CO_2 source(s) (**Figure 8**). If methanogenesis of soil organic matter (OM) occurs in the saturated phreatic zone, where a high watertable maintains a closed system under seasonally wet conditions, it may generate a source of carbonate with more negative $\delta^{13}C_{VPDB}$ values that could result in a more negative stable-carbon isotopic value of the micrite and microspar cements. These negative $\delta^{13}C$ values are a mixture of CO_2 and CH_4 derivation (**Figure 8A**). The soil uptake of, and interchange with, atmospheric CO_2 under these circumstances remains in the overlying vadose zone, without contribution of that carbon source to the resultant $\delta^{13}C$ values

TABLE 1 | Mean $\delta^{13}C_{VPDB}$ and $\delta^{18}O$ values of pedogenic nodule-calcite cements obtained from intraformational conglomerate deposits, with GPS coordinates, and stratigraphic positions across the area from Old Lootsberg Pass to Tweefontein[2] (**Figure 4**).

Sample	Latitude	Longitude	$\delta^{13}C_{VPDB}$ (‰)	$\delta^{18}O_{VPDB}$ (‰)	$\delta^{18}O_{VSMOW}$ (‰)	N
P61 PNC	31.79462	24.80632	4.53	15.07	15.33	2
WP873	31.8076	24.82387	7.09	16.74	13.61	2
WP871	31.79545	24.80642	5.47	18.62	11.67	2
P51	31.79505	24.79875	2.13	16.56	13.79	6
Datum	31.79618	24.79635	9.435	21.27	8.93	2
WP878	31.836	24.8483	4.78	16.49	13.86	4
WP870	31.79649	24.80576	11.01	20.20	10.04	4
WP879	31.83609	24.84832	4.48	16.32	14.04	4
WP877	31.83629	24.84811	11.26	18.44	11.85	3
WP857	31.83276	24.84477	4.27	15.09	15.30	4
WP863	31.83268	24.84374	9.49	16.02	14.35	4
WP864	31.83271	24.8436	8.58	15.91	14.46	4
WP848	31.83273	24.84355	5.21	17.25	13.08	5
WP843	31.83327	24.84063	6.82	15.13	15.26	3

of the soil-nodule cement. The closed nature of the system and contribution of CO_2 derived from methanogenic bacteria results in micrite and microspar cement $\delta^{13}C_{VPDB}$ values lower than −12.1‰ (**Figure 8A**; Gastaldo et al., 2014). In contrast, calcite in well-drained soils precipitates under open-system, one-dimensional, Fickian-type diffusive mixing of atmospheric CO_2 and CO_2 derived from *in situ* oxidation of soil OM (**Figure 8C**; Cerling, 1991). Under these conditions, soil-formed calcite $\delta^{13}C_{VPDB}$ values will be more positive than coexisting OM $\delta^{13}C$ values. This results from a 4.4‰ ^{13}C enrichment associated with diffusive transport of biologically derived CO_2 (Cerling, 1991), and temperature-dependent carbon-isotope enrichment associated with carbon-isotope fractionation between carbonate species (Romanek et al., 1992; see full discussion in Gastaldo et al., 2014). Micrite and microspar cements precipitated under these conditions of open-system exchange will have a $\delta^{13}C_{VPDB}$ value that is higher than −8.3‰. Values between −8.3 and −12.1‰ may, or may not, have crystallized in soils characterized by one-dimensional CO_2 diffusion. Cements exhibiting these intermediate values are interpreted to represent precipitation in a soil that possibly reflects well-drained conditions, or one that experienced a variable watertable over time (**Figures 8B**, 9; Gastaldo et al., 2014). Unless diagenetically altered, $\delta^{13}C$ values of micrite and microspar cements in soil nodules are fixed and provide insight into the conditions under which they formed, whether found *in situ* in a calcic Vertisol (Gastaldo et al., 2020b) or as reworked recalcitrant residuum in fluvial channel-lag deposits (Pace et al., 2009; Gastaldo et al., 2018).

Generalized $\delta^{13}c$ and $\delta^{18}o$ Landscape Model

Cycles of floodplain/landscape accumulation (aggradation) and erosion and reworking (degradation) are controlled by changes in fluvial gradient of a basin, which are influenced by a variety of factors over time including climate (Bull, 2009; Gastaldo and Demko, 2011). High rates of floodplain aggradation occur in a part of a basin, but not contemporaneously throughout a basin, when the regional fluvial gradient is in disequilibrium. Disequilibrium results in landscape erosion in the more proximal source areas of the basin. Erosion, there, results in higher suspension-load and bedload sediment in rivers, which is deposited distally in the receiving area. Overbank deposits are rooted by plants (all considered to be C3 photosynthetic plants in the Permian–Triassic; Osborne and Beerling, 2006) and colonized by invertebrates, with the mean regional watertable controlled, in part, by base level of river systems traversing the floodplains (**Figure 9A**). Organic matter is contributed to poorly developed soils (e.g., Inceptisols, Entisols) through the aerobic bacterial recycling of aerial and subterranean plant parts, surficial and subsurface fungal degradation, and excrement from herbivorous and burrowing animal activities.

During an aggradational phase, overbank sedimentation is common, soil thickness increases across the interfluves, and there is a concomitant rise in regional watertable. Residual OM of previous soil profiles becomes part of the phreatic zone where continued decay is promoted and controlled by anaerobic processes including methanogenesis (**Figure 9B**). The liberation of both CO_2 and CH_4 into pore waters (the $\delta^{18}O$ values of which reflect meteoric contribution) surrounding the decaying OM may react with available metal cations and precipitate calcite in the form of micrite. Fine-grained sediment is cemented into a nodule around an organic nucleus. The size of these early diagenetic nodules is dependent on a number of factors including the original size of the organic nucleus (disseminated detritus vs. articulated skeleton at different ends of the preservational spectrum), the concentration of cations in the pore waters, and the stability of the phreatic zone over time. $\delta^{13}C_{VPDB}$ values of calcite cements in nodules and concretions formed under these saturated conditions are < –12.1‰ and are interpreted as reflecting closed-system, poorly drained soil conditions in the Permian–Triassic Karoo Basin (Tabor et al., 2007). One factor sustaining poorly drained soil conditions is the prevalence of a seasonally wet climate, where the number of wet months exceeds

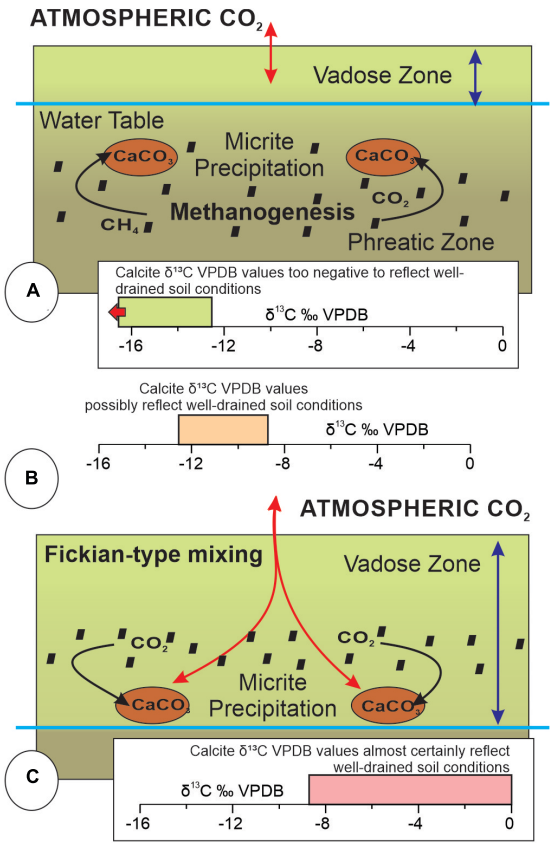

FIGURE 8 | End-member diagram showing the relationship between $\delta^{13}C$ values of calcite cement in pedogenic nodules formed under closed and open systems. **(A)** $\delta^{13}C_{VPDB}$ values < −12.1‰ reflect calcite precipitation under saturated soil conditions in the phreatic zone with carbon contribution from anaerobic decay of organic matter (Tabor et al., 2007; Gastaldo et al., 2014). Carbon contribution to the soil is restricted to the overlying vadose zone and plays no role in, or has no influence on, the $\delta^{13}C$ values of calcite cements. **(B)** $\delta^{13}C_{VPDB}$ values between < −12.1 and −8.3‰ reflect calcite precipitation with contributions from both methanogenic and atmospheric carbon sources. **(C)** $\delta^{13}C_{VPDB}$ values > −8.3‰ reflect calcite precipitation under open soil conditions forming in the lower soil horizons at the terminus of the wetting front, the interface between the vadose and phreatic zones. Carbon contribution primarily from atmospheric sources.

the number of dry months (rainfall exceeds evapotranspiration; Cecil and Dulong, 2002). Moister and/or cooler regions tend to have lower (more negative) meteoric water (e.g., Craig, 1961) and carbonate (Cerling, 1984; Cerling and Quade, 1993) $\delta^{18}O$ values than warmer and drier regions.

Changes in the regional fluvial gradient, sediment supply to the drainage system, or climate toward more seasonally dry or monsoonal conditions will result in a slowing of floodplain aggradational rate. Vegetation will continue to colonize the floodplains, adding OM to the soil in lower quantities than under more seasonally wet or everwet conditions (Gastaldo, 1994). A lower regional watertable, as a consequence of greater variance in seasonal base level, allows for atmospheric gasses to interact in the vadose zone over a longer yearly time frame. Tropospheric CO_2 mixes with methanogenic carbon sources during calcite crystallization, resulting in more positive $\delta^{13}C_{VPDB}$ values of fine-grained carbonate cements ranging between −12.1 and −8.3‰ (**Figure 9C**). There is an accompanying shift to more positive $\delta^{18}O$ values that may be related to warming, reduced precipitation, and evaporative ^{18}O enrichment (Tabor et al., 2002). In addition to tectonic influences such as changes in regional gradient, aggradation may also be halted when overall climate becomes increasingly seasonally dry (evapotranspiration exceeds rainfall; Cecil and Dulong, 2002). Under these conditions, the landscape remains in a static phase, or stasis. Base level is low and fluvial channels may be dry for several months, accompanied by an overall lowering of the regional watertable (**Figure 9D**). A shift to a relative increase in the contribution of an atmospheric CO_2 source for calcite precipitation results in $\delta^{13}C_{VPDB}$ values greater than −8.3‰ in nodule cement, and more positive $\delta^{18}O_{VSMOW}$ values driven by ^{18}O evaporative enrichment. A swing in climate to more seasonally wet or everwet conditions, accompanied by some change in fluvial gradient, begins a phase of erosion, landscape degradation, and reworking of floodplain soils.

The degradational phase of the cycle removes and remobilizes the fine clastic component, placing this grain-size fraction in suspension load and transporting it further basinward where it is redeposited. Depending on the competence and carrying capacity of the fluvial system, the coarser soil fractions–peds and soil aggregates (Gastaldo et al., 2013), euhedral pyrite where soil conditions were present to promote its formation (Gastaldo et al., 2020b), and calcite-cemented glaebules, nodules, and concretions–also may be displaced further basinward or concentrated as lag deposits in local channels (**Figure 9E**). Within this conceptual model for the formation of PNC units, channel lags of pedogenic nodules represent a time-averaged deposit of detrital pedogenic materials. The stable isotopic composition of individual clasts (i.e., pedogenic nodules) represents one or more paleoclimate signals of the eroded soil or stacked soil profiles. Where the carbon- and oxygen-stable isotope composition of nodules from a PNC exhibit a narrow range, the signal likely represents one or more eroded soils in which the nodules formed under a relatively limited set of climatic conditions. Where the range of isotopic values is wider, the signal likely represents the erosion of one or more soils, each of which may have formed under different climatic conditions or disparate environments (e.g., alternating episodes of poorly drained and well drained during which time pedogenic carbonate is forming). It is also possible that these values represent the erosion of a compound and/or composite soil profile (Gastaldo et al., 2020b). Nevertheless, the paleoclimate signal recovered from pedogenic nodules concentrated in channel-lag deposits represents a part of the sedimentary succession that is no longer present in the stratigraphy and cannot be sampled, directly. This residuum represents one or more "ghost" landscapes.

Stable-Isotope Trends of Eroded Landscapes at Old Lootsberg Pass

The 55 analyses of nodules sampled from fourteen PNC channel-lag deposits distributed over more than 200 m of measured

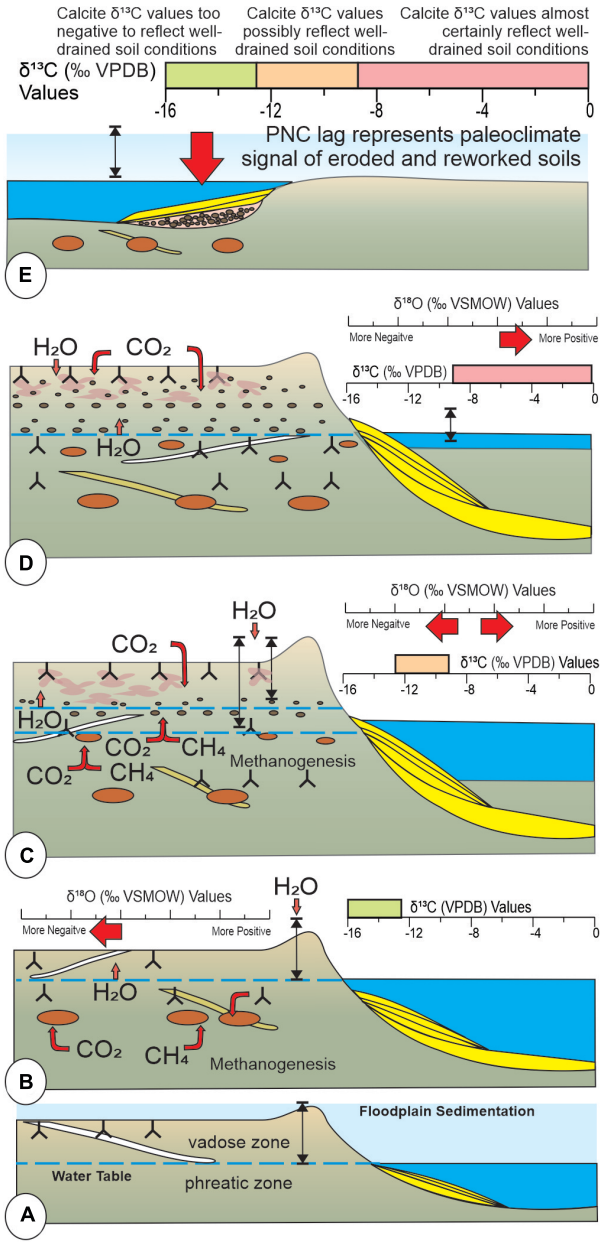

FIGURE 9 | Generalized aggradational/degradational landscape model coupling the phase of interfluve development, water-table, carbon source for calcite cement, and $\delta^{13}C$ and $\delta^{18}O$ values associated with pedogenic calcite-cemented nodules formed under these parameters (after Gastaldo et al., 2020b). **(A)** Initial aggradational phase with rooting and invertebrate bioturbation of the upper soil horizons accompanying overbank deposition. **(B)** Second phase of floodplain aggradation where rate of overbank deposition is high. Immature soils are buried in the phreatic zone due to a rise in watertable. Anaerobic decay of organic matter releases both CO_2 and CH_4 into pore waters, adding HCO_3 and modifying acidity, promoting calcite precipitation around organic nucleus. Values of both $\delta^{13}C$ and $\delta^{18}O$ of calcite cements are more negative. **(C)** Third phase of overbank aggradation with a reduced frequency of overbank deposition and greater seasonality. Pedogenesis over longer time scales and greater variance in seasonal rainfall results in greater flux and penetration of the watertable, affecting $\delta^{13}C$ and $\delta^{18}O$ values of calcite cements. $\delta^{13}C$ values reflect precipitation possibly

(Continued)

FIGURE 9 | Continued

under well-drained conditions, whereas values of $\delta^{18}O$ fall between end members. **(D)** The fourth landscape phase is one of stasis, when sediment supply to the floodplains is minimal as a consequence of a warmer and more seasonally dry climate with infrequent overbank deposition. Watertable is low, soil mottling is common, and pedogenic nodule cement precipitates in equilibrium with tropospheric gasses that penetrate deep into the soil profile. Both $\delta^{13}C$ and $\delta^{18}O$ values are more positive, reflecting crystallization under well-drained soil conditions. **(E)** A change in fluvial equilibrium and a shift to more seasonally wet climate results in floodplain erosion, scavenging of interfluvial deposits, and concentration of larger clasts in intraformational channel-lag conglomerate above erosional surfaces. $\delta^{13}C$ and $\delta^{18}O$ values of pedogenic nodules from these deposits represent the spectrum of paleoclimate signals of these "ghost" horizons.

stratigraphic section, with the benefits of geochronometric and paleomagnetic context in a stratigraphic framework (Gastaldo et al., 2018; **Figure 4**), exhibit a similar variance of values above individual erosional boundaries (**Figure 7**). There is also a positive correlation in excursions upsection of $\delta^{13}C$ and $\delta^{18}O$ values of calcite cement toward heavier values (**Figure 10**). Two distinct clusters of pedogenic carbonate stable carbon- and oxygen-isotope values occur in these data.

Eight of the fourteen PNC beds cluster in a narrow stable-isotope range of $< 2.5‰$, whereas the remaining samples from other PNC horizons exhibit a wide range of, or bimodal (**Figure 7**), variance in values. There are three intervals in which the stable-isotope values of successive sampled PNC layers fall in a tight range. The most pronounced of these occurs in the middle of the succession–PNC beds WP848, WP879, WP878–where the average $\delta^{13}C_{VPDB}$ and $\delta^{18}O_{VSMOW}$ values are -5.2 and $13.1‰$, -4.5 and $14.0‰$, and -4.8 and $13.9‰$, respectively (**Figure 10**). We interpret these, and similar, $\delta^{13}C$ values to reflect calcite precipitation under an open system with contribution of atmospheric CO_2 as one of the sources of carbonate for pedogenic micrite crystallization (Gastaldo et al., 2014). The paleosols from which these nodules originated are interpreted to have formed under well-drained soil conditions. The positive $\delta^{18}O$ values derived from calcite cement of these samples are indicative of conditions that were seasonally warmer and drier, with higher evapotranspiration and, likely, a greater number of dry than wet months (Sikes and Ashley, 2007).

In contrast, the second sample group exhibits a wider range of stable-isotope values (**Figure 7**), and two of these PNC beds, or conglomeratic lag deposits, appear to be associated with intervals where more negative $\delta^{13}C$ values of nodular micrite are found (**Figure 10**). The average $\delta^{13}C_{VPDB}$ values in this clutch of samples range from $-11.3‰$ (WP877) to $-8.6‰$ (WP864), and the soils from which these PNC layers originate are interpreted to have developed possibly under well-drained conditions because of these calcite $\delta^{13}C$ values (Gastaldo et al., 2014). The most negative $\delta^{13}C_{VPDB}$ values in this sample cohort are $< -12.8‰$, indicating calcite crystallization under a poorly drained, closed-system, soil-forming environment (Tabor et al., 2007). As evidenced by the extreme range in $\delta^{13}C$ values, pedogenic nodules hosted in this sample group either originated from two or more eroded soils, or may have originated from a compound,

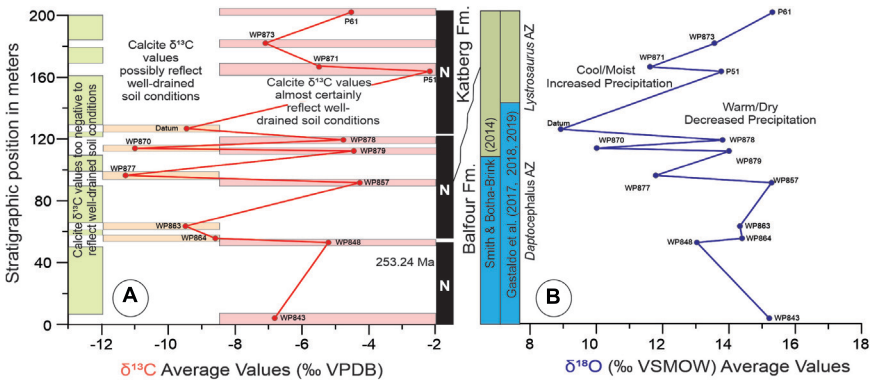

FIGURE 10 | Stratigraphic trends of mean values of δ^{13}_{CVPDB} **(A)** and δ^{18}_{OVSMOW} **(B)** derived from pedogenic nodules formed in "ghost" landscapes plotted against published magnetostratigraphy (Gastaldo et al., 2018) and models of vertebrate biostratigraphy in geochronometric context (Gastaldo et al., 2015) demonstrating cyclicity in seasonally wet (represented by green rectangles) and seasonally dry landscapes (represented by orange and reddish rectangles). This trend is similar to that at Wapadsberg Pass (Gastaldo et al., 2014, 2020b) and shows an overall wetting trend towards the boundary between the *Daptocephalus* and *Lystrosaurus* AZs rather than a unidirectional warming as reported by other workers (Ward et al., 2005; Smith and Botha-Brink, 2014; Rey et al., 2016; Botha et al., 2020).

composite (time averaged) soil interval(s) as documented in the *Daptocephalus* AZ near Wapadsberg Pass (Gastaldo et al., 2020b) or in the *Lystrosaurus declivis* AZ in another part of the basin (Harrison et al., 2018). Lower $\delta^{18}O$ values from these horizons are interpreted to indicate seasonally cooler and wetter conditions at the time of calcite-nodule formation. Similar $\delta^{18}O$ values are reported by Rowe and Maher (2000) in the Loess Plateau of north-central China, Neymark et al. (2005) in Crater Flat, Nevada, United States, where cool/cold climatic conditions prevail (MAT 15° C), and Schmid et al. (2006) at depth in soil profiles of the Broken Hill region of Australia, used to interpret colder conditions than at present. We also note that our data set overlaps that presented by Viglietti et al. (2013) from two *Lystrosaurus* bone beds on the Donald 207 (Fairydale) farm, reported in the *L. declivis* Assemblage Zone, and interpreted to have formed under a semi-arid and seasonally cold climate.

Shifts in the drier "ghost" landscape intervals at Old Lootsberg Pass reflect changes in meteoric precipitation amounts and relative temperature in the latest Permian *Daptocephalus* and *Lystrosaurus declivis* Assemblage Zones (**Figure 10**). These trends contrast with the wetter aggradational phases in which both macrofloral and microfloral assemblages are preserved (Gastaldo et al., 2005, 2017, 2019; DiMichele and Gastaldo, 2008) in greenish to reddish-gray siltstone (Li et al., 2017), associated with the seasonally wet *Katbergia* ichnofauna (**Figure 4**; Gastaldo and Rolerson, 2008). Assuming that the controls over the intervals dominated by a seasonally wet climate were similar (**Figure 10**), the late Changhsingian succession at Old Lootsberg Pass exhibits a wet/dry cyclicity that may have been in consort with astronomically driven obliquity and precession cycles recognized in the latest Permian marine record (e.g., Huang et al., 2011; Wu et al., 2013; Li et al., 2016).

A widely accepted paradigm for the transitioning conditions across the *Daptocephalus* to *Lystrosaurus declivis* boundary is one of increasing aridity and temperature (MacLeod et al., 2000, 2017; Ward et al., 2005; Smith and Botha-Brink, 2014; Rey et al., 2016; Botha et al., 2020). But, the PNC stable-isotope trend presented here from Old Lootsberg Pass, which is a similar record to that previously identified at Wapadsberg Pass less than 16 km to the southeast (Gastaldo et al., 2014, 2020b), shows increasingly moist and cool conditions toward the biozone boundary, as currently defined (Smith and Botha-Brink, 2014; Botha and Smith, 2020; Viglietti, 2020). The paleosol profiles from which pedogenic calcite-cemented nodules originated may not have been as extremely dry as envisioned or interpreted from the vertebrate $\delta^{18}O_{VSMOW}$ apatite record (MacLeod et al., 2000, 2017; Botha et al., 2020).

There are very few paleosol profiles in the *Daptocephalus* AZ in which small, calcite-cemented nodules are found *in situ*. Neveling et al. (2016b) identified one interval in the Old Lootsberg Pass section that underlies an erosional fluvial contact where a well-developed lateral channel bar is preserved without a PNC lag. Pedogenic nodules scavanged from the underlying soil horizon, when cut out by the laterally equivalent channel, must have concentrated in other parts of this particular fluvial channel elsewhere in the region. The PNC-bearing siltstone paleosol is 1.5 m in thickness and exposed over < 5 m of lateral distance in which small, cm-diameter carbonate-cemented nodules and carbonate-cemented, subvertical-to-subhorizontal, mm-scale tubules are dispersed throughout. Neither horizonation, color differentiation, nor pedogenic evidence to discriminate soil profiles are discernible in the field at this site.

Another record of *in situ* soils includes a succession of Stage II calcic Vertisols in the upper *Daptocephalus* AZ and is exposed in an erosional gully (donga) adjacent to an 11-m thick channel cutout on farm Quaggasfontein in the Old Wapadsberg Pass area (farm 527/Quaggasfontein; Gastaldo et al., 2020b). Here, one compound-composite soil interval has been characterized in detail, and provides some insight into the climate under which these nodules formed. The geochemical data from the 527/Quaggasfontein Vertisol include TOC, LOI, and concentrations of selected major and minor elements using inductively coupled plasma-mass spectrometry [ICP-AES and

ICP-MS (zircon)]. Molecular weathering-ratios, including base loss, clayeyness, mineral assemblage stability (MAS), calcification, salinization, and the chemical index of alteration minus potassium (CIA-K), were calculated. Bulk-rock geochemical data also were evaluated using a mass-balance approach and Ti as the immobile element. Using molar ratios of CIA-K and salinization, respectively, provide proxy estimates of MAP and MAT (Sheldon and Tabor, 2009) during this time of Late Permian pedogenesis. Gastaldo et al. (2020b) provide estimates for MAT = 10.2 ± 4.4°C and MAP = 1,083 ± 181 mm/yr from data that were collected from a carbonate nodule-bearing paleosol. Hence, rather than pedogeneis and precipitation of calcite-cemented nodules under a hot and arid climate (< 2.5 months of precipitation under which Aridisols develop; Cecil and Dulong, 2002), these Vertisols developed under a more seasonally dry set of cool conditions in which values of $\delta^{13}C_{VPDB}$ micrite cements of *in situ* pedogenic nodules range from −8.6 to −5.4‰. The $\delta^{13}C$ values at Old Lootsberg Pass to Tweefontein and near Old Wapadsberg Pass (527/Quaggasfontein) indicate that the Late Permian landscape experienced episodically wet and episodically dry phases that alternated in both the *Daptocephalus* and *Lystrosaurus declivis* AZs without evidence for a unidirectional drying of the landscape over this interval of time.

CONCLUSION

The latest Permian stratigraphy of the Karoo Basin, South Africa, is a discontinuous record dominated by successions of aggradational continental (fluvial, interfluvial, and rarely lacustrine) deposits punctuated by erosional surfaces marking periods of landscape degradation. Aggradational floodplain greenish-gray and reddish-gray siltstone mainly represent interfluvial paleosols, interspersed with localized abandoned fluvial channel-fill (thicker sandstone beds and interbedded heterolithic facies) sedimentary successions. Aggradational floodplain soils consist primarily of poorly developed Inceptisols and, rarely, Vertisols in which calcite-cemented *in situ* pedogenic nodules may have formed. It is not that more seasonally dry soils were rare in the latest Permian. Rather, evidence of their existence is found most commonly in the form of intraformational conglomerate at the base of channels that had eroded and reworked them, concentrating the more resilient clasts in lag deposits above an erosional surface. That erosional surface marks a period of landscape degradation and the removal of the more seasonally dry landscapes from the observable stratigraphy. Yet, it is possible to garner paleoclimate proxy data from the detrital, sedimentary remains of these "ghost" soils, even in their absence as paleosol profiles in the physical stratigraphic record. This can be accomplished by analyzing unaltered calcite of pedogenic nodule cements preserved in PNC beds of the uppermost Balfour and lowermost Katberg formations.

Pedogenic calcite-cemented nodules from fourteen intraformational conglomerates, sampled over ∼200 m of stratigraphic section in the Eastern Cape Province, provide a $\delta^{13}C$ and $\delta^{18}O$ data set from which paleoclimate trends are evaluated through the deposition of the upper *Daptocephalus* and lower *Lystrosaurus declivis* AZs. The transition across, and reported loss of vertebrate biodiversity between these biozones has been interpreted as the consequence of a unidirectional trend toward increasing aridity and rising temperature (Ward et al., 2005; Smith and Botha-Brink, 2014; Botha et al., 2020). The basic stratigraphic model that characterizes the uppermost *Daptocephalus* and basal *Lystrosaurus declivis* AZs, as currently defined, with rare PNCs bounding thicker aggradational packages at the base, indicate that the later Permian landscapes were subjected to alternating wet-and-dry phases. Stable-isotope data representing the "ghost" landscapes over the 11 measured stratigraphic sections, reported herein, and correlated across an area of > 5 km laterally from Old Lootsberg Pass to Tweefontein[2], document climate variation or shifts in the proxy records of the more seasonally dry intervals. Mean $\delta^{13}C_{VPDB}$ values range from −11.3‰ to −8.6 in nodules formed under possibly well-drained soil conditions, with $\delta^{18}O_{VSMOW}$ values from 8.9 to 14.1‰ indicating that the climate was cool and moist. Mean $\delta^{13}C_{VPDB}$ values range from −7.1 to −2.1‰ in nodules formed in well-drained soils, with $\delta^{18}O_{VSMOW}$ values from 11.6 to 15.3‰ indicating that the climate was relatively warmer and drier. Trends in $\delta^{13}C$ and $\delta^{18}O$ values are correlated, and an oscillation between seasonally wet and seasonally dry landscapes characterize both the upper *Daptocephalus* and lower *Lystrosaurus declivis* AZs. This observation is similar to the one reported by Gastaldo et al. (2020b) in the Wapadsberg Pass area, ∼16 km from Old Lootsberg Pass. Yet, the overall trend in climate proxies leading up to the boundary between vertebrate biozones appears to be one of increasing cool and moist soil conditions, rather than of increasing warmth and dryness. The $\delta^{13}C$ and $\delta^{18}O$ values obtained above the biozone boundary broadly overlap those reported lower in the succession without any discernible trend. Our findings are in contrast to those reported by other workers based on the $\delta^{13}C$ and $\delta^{18}O$ values obtained from vertebrate-tusk apatite. Hence, we find no evidence from soil nodules to support a unidirectional increase in temperature and aridity approaching the biozone boundary, which some authors have equated to the end-Permian marine crisis, in these classic continental sections that are foundational to the terrestrial extinction paradigm.

DATA AVAILABILITY STATEMENT

The raw data supporting the conclusions of this article will be made available by the authors, without undue reservation.

AUTHOR CONTRIBUTIONS

RG and JN measured all stratigraphic sections, collected PNC samples for analyses, and were responsible for tracing major sandstone bodies, used as correlation datums across the escarpment, and developed the stratigraphic framework into which the following analyses are placed. NT undertook stable carbon-and-oxygen isotopic analyses and, in collaboration with RG, interpreted these data in stratigraphic context. All authors contributed to the article and approved the submitted version.

FUNDING

Research efforts were supported, in part, by: the Council for Geoscience (South Africa); National Science Foundation of the United States EAR 0749895, 0934077, 1123570 and 1624302; and a Fulbright Scholar Award from the U.S. Department of State to RG.

ACKNOWLEDGMENTS

We would like to thank the following colleagues for field-and-laboratory assistance: Dr. K. Andrzejewski, SMU; Ms. K. Kus and Mr. S. Sinkler, Colby College; and Ms. Sisanda Makubalo, Council for Geoscience. We appreciate the hospitality and kindness shown to us over the past decade by: Justin and Liesl Kingwill, Blaauwater Farm; and JP and Hester Steynberg, Ganora Guest Farm.

SUPPLEMENTARY MATERIAL

The Supplementary Material for this article can be found online at: https://www.frontiersin.org/articles/10.3389/fevo.2020.567109/full#supplementary-material

REFERENCES

Benton, M. J., and Newell, A. J. (2014). Impacts of global warming on Permo-Triassic terrestrial ecosystems. *Gondwana Res.* 25, 1308–1337. doi: 10.1016/j.gr.2012.12.010

Bernardi, M., Petti, F. M., and Benton, M. J. (2018). Tetrapod distribution and temperature rise during the Permian–Triassic mass extinction. *Proc. R. Soc. B Biol. Sci.* 285:20172331. doi: 10.1098/rspb.2017.2331

Botha, J., Huttenlocker, A. K., Smith, R. M. H., Prevec, R., Viglietti, P., and Modesto, S. P. (2020). New geochemical and palaeontological data from the Permian-Triassic boundary in the South African Karoo Basin test the synchronicity of terrestrial and marine extinctions. *Palaeogeogr. Palaeoclimatol. Palaeoecol.* 540:109467. doi: 10.1016/j.palaeo.2019.109467

Botha, J., and Smith, R. H. M. (2006). Rapid vertebrate recuperation in the Karoo Basin of South Africa following the End-Permian extinction. *J. Afr. Earth Sci.* 45, 502–514. doi: 10.1016/j.jafrearsci.2006.04.006

Botha, J., and Smith, R. M. H. (2020). Biostratigraphy of the *Lystrosaurus* assemblage zone (Beaufort Group, Karoo Supergroup), South Africa. *S. Afr. J. Geol.* 123, 207–216. doi: 10.25131/sajg.123.0015

Broom, R. (1906). On the permian and triassic faunas of South Africa. *Geol. Magaz.* 3, 29–30. doi: 10.1017/s001675680012271x

Broom, R. (1911). On some New South African permian reptiles. *Proc. Zool. Soc. Lond.* 81, 1073–1082. doi: 10.1111/j.1096-3642.1911.tb01976.x

Bull, W. (2009). *Geomorphic Responses to Climatic Change*. Caldwell, NJ: The Blackburn Press.

Catuneanu, O., Wopfner, H., Eriksson, P. G., Cairncross, B., Rubidge, B. S., Smith, R. M. H., et al. (2005). The Karoo basins of south-central Africa. *J. Afr. Earth Sci.* 43, 211–253. doi: 10.1016/j.jafrearsci.2005.07.007

Cecil, C. B., and Dulong, F. T. (2002). "Precipitation models for sediment supply in arm climates," in *Climate Controls on Stratigraphy*, eds C. G. Cecil and N. T. Edgar (Tulsa: SEPM), 21–27. doi: 10.2110/pec.03.77.0021

Cerling, T. E. (1984). The stable isotopic composition of modern soil carbonate and its relationship to climate. *Earth Planet. Sci. Lett.* 71, 229–240. doi: 10.1016/0012-821x(84)90089-x

Cerling, T. E. (1991). Carbon dioxide in the atmosphere: evidence from Cenozoic and Mesozoic paleosols. *Am. J. Sci.* 291, 377–400. doi: 10.2475/ajs.291.4.377

Cerling, T. E., and Quade, J. (1993). "Stable carbon and oxygen isotopes in soil carbonates," in *Climate Change in Continental Isotopic Records. Geophysics Monograph*, eds J. A. McKenzie and S. Savin (Washington, DC: American Geophysical Union), 217–231. doi: 10.1029/gm078p0217

Craig, H. (1957). Isotopic standards for carbon and oxygen and correction factors for mass-spectrometric analysis of carbon dioxide. *Geochim. Cosmochim. Acta* 12, 133–149. doi: 10.1016/0016-7037(57)90024-8

Craig, H. (1961). Isotopic variations in meteoric waters. *Science* 133, 1702–1703. doi: 10.1126/science.133.3465.1702

Day, M. O., Ramezani, J., Bowring, S. A., Sadler, P. M., Erwin, D. H., Abdala, F., et al. (2015). When and how did the terrestrial mid-Permian mass extinction occur? Evidence from the tetrapod record of the Karoo Basin, South Africa. *Proc. R. Soc. B* 282:20150834. doi: 10.1098/rspb.2015.0834

De Kock, M. O., and Kirschvink, J. L. (2004). Paleomagnetic constraints on the permian-triassic boundary in terrestrial strata of the karoo supergroup, South Africa: implications for causes of the end-permian extinction event. *Gondwana Res.* 7, 175–183. doi: 10.1016/s1342-937x(05)70316-6

Deutz, P., Montanez, I. P., Monger, H. C., and Morrison, J. (2001). Morphology and isotope heterogeneity of Late Quaternary pedogenic carbonates: implications for paleosol carbonates as paleoenvironmental proxies. *Palaeogeogr. Palaeoclimatol. Palaeoecol.* 166, 293–317. doi: 10.1016/s0031-0182(00)00214-5

DiMichele, W. A., and Gastaldo, R. A. (2008). Plant paleoecology in deep time. *Ann. Missouri Bot. Gardens* 95, 144–198. doi: 10.3417/2007016

Ekart, D. D., Cerling, T. E., Montañez, I. P., and Tabor, N. J. (1999). A 400 million year carbon isotope record of pedogenic carbonate: implications for paleoatmospheric carbon dioxide. *Am. J. Sci.* 299, 805–827. doi: 10.2475/ajs.299.10.805

Freytet, P., and Plaziat, J. C. (1982). Continental carbonate sedimentation and pedogenesis–Late Cretaceous and Early Tertiary of southern France. *Contribut. Sedimentol.* 12, 1–213.

Gastaldo, R. A. (1994). "The genesis and sedimentation of phytoclasts with examples from coastal environments," in *Sedimentation of Organic Particles*, ed. A. Traverse (Cambridge, MA: Cambridge University Press), 103–127. doi: 10.1017/cbo9780511524875.008

Gastaldo, R. A., Adendorff, R., Bamford, M. K., Labandeira, Neveling, J., and Sims, H. J. (2005). Taphonomic trends of macrofloral assemblages across the permian-triassic boundary, Karoo Basin, South Africa. *PALAIOS* 20, 478–497. doi: 10.1016/j.palaeo.2010.03.052

Gastaldo, R. A., and Demko, T. M. (2011). Long term hydrology controls the plant fossil record. *Top. Geobiol.* 32, 249–286. doi: 10.1007/978-90-481-8643-3_7

Gastaldo, R. A., Kamo, S. L., Neveling, J., Geissman, J. W., Bamford, M., and Looy, C. V. (2015). Is the vertebrate defined Permian–Triassic Boundary in the Karoo Basin, South Africa, the terrestrial expression of the End Permian marine event? *Geology* 43, 939–942. doi: 10.1130/G37040.1

Gastaldo, R. A., Knight, C. L., Neveling, J., and Tabor, N. J. (2014). Latest Permian paleosols from Wapadsberg Pass, South Africa: implications for Changhsingian climate. *Geol. Soc. Am. Bull.* 126, 665–679. doi: 10.1130/B30887.1

Gastaldo, R. A., Kamo, S. L., Neveling, J., Geissman, J., Looy, C. V., and Martini, A. M. (2020a). The base of the *Lystrosaurus* assemblage zone, Karoo Basin, predates the end-Permian marine extinction: age and paleomagnetic evidence. *Nat. Commun.* 11:1428. doi: 10.1038/s41467-020-15243-7

Gastaldo, R. A., Kus, K., Neveling, J., and Tabor, N. J. (2020b). Calcic vertisols in the upper *Daptocephalus* assemblage zone, balfour formation, Karoo Basin, South Africa: implications for late permian climate. *J. Sediment. Res.* 90, 609–628. doi: 10.2110/jsr.2020.32

Gastaldo, R. A., Neveling, J., Geissman, J. W., and Kamo, S. L. (2018). A lithostratigraphic and magnetostratigraphic framework in a geochronologic context for a purported Permian–Triassic boundary section at Old (West) Lootsberg Pass, Karoo Basin, South Africa. *Geol. Soc. Am. Bull.* 130, 1411–1438. doi: 10.1130/b31881.1

Gastaldo, R. A., Neveling, J., Geissman, J. W., and Li, J. W. (2019). A multidisciplinary approach to review the vertical and lateral facies relationships

of the purported vertebrate-defined terrestrial boundary interval at bethulie, Karoo Basin, South Africa. *Earth Sci. Rev.* 189, 220–243. doi: 10.1016/j.earscirev.2017.08.002

Gastaldo, R. A., Neveling, J., Looy, C. V., Bamford, M. K., and Kamo, S. L. (2017). Paleontology of the Blaauwater 67 and 65 farms, South Africa: testing the *Daptocephelus/Lystrosaurus* biozone boundary in a stratigraphic framework. *PALAIOS* 32, 349–366. doi: 10.2110/palo.2016.106

Gastaldo, R. A., Pludow, B. A., and Neveling, J. (2013). Mud aggregates from the Katberg Formation, South Africa: additional evidence for Early Triassic degradational landscapes. *J. Sediment. Res.* 83, 531–540. doi: 10.2110/jsr.2013.45

Gastaldo, R. A., and Rolerson, M. W. (2008). *Katbergia* gen. nov., A new trace fossil from the Upper Permian and Lower Triassic Rocks of the Karoo Basin: implications for paleoenvironmental conditions at the P/Tr extinction event. *Palaeontology* 51, 215–229. doi: 10.1111/j.1475-4983.2007.00743.x

Gonfiantini, R. (1984). Stable isotope reference samples for geochemical and hydrological investigations. *Int. J. Appl. Radiat. Isotopes* 35:426. doi: 10.1016/0020-708x(84)90059-0

Groenewald, G. H. (1996). *Stratigraphy and sedimentology of the Tarkastad Subgroup, South Africa*. Unpublished PhD thesis, University of Port Elizabeth, Summerstrand.

Grossman, E. L., Mii, H.-S., Zhang, C., and Yancey, T. E. (1996). Chemical variation in Pennsylvanian brachiopod shells: diagenetic, taxonomic, microstructural, and seasonal effects. *J. Sediment. Res.* 66, 1011–1022.

Harrison, S. D., Gastaldo, R. A., and Neveling, J. (2018). *Testing for Carbonate-rich Paleosols in the Lower Lystrosaurus Assemblage Zone, Karoo Basin, South Africa*. Boulder, CO: Geological Society of America.

Huang, C., Tong, J., Hinnov, L. A., and Chen, Z.-Q. (2011). Did the great dying of life take 700 k.y. Evidence from global astronomical correlation of the Permian-Triassic boundary interval. *Geology* 39, 779–782. doi: 10.1130/G32126.1

Johnson, M. R. (1976). *Stratigraphy and sedimentology of the Cape and Karoo sequences in the Eastern Cape Province*. Unpublished PhD thesis, Rhodes University, Grahamstown.

Johnson, M. R., van Vuuren, C. J., Visser, J. N. J., Cole, D. I., de Wickens, H. V., Christie, A. D. M., et al. (2006). "Sedimentary rocks of the Karoo Supergroup," in *The Geology of South Africa. Geological Society of South Africa*, eds M. R. Johnson, C. R. Anhaeusserm, and R. J. Thomas (Pretoria: Johannesburg, Council for Geoscience), 461–479.

Keyser, A. W. (1979). A review of the biostratigraphy of the beaufort group in the Karoo Basin of South Africa. *Geol. Soc. S. Afr.* 2, 13–31.

Keyser, A. W., and Smith, R. H. M. (1978). Vertebrate biozonation of the beaufort group with special reference to the Western Karoo Basin. *Ann. Geol. Surv.* 12, 1–35.

Kitching, J. W. (1971). "A short review of the Beaufort zoning in South Africa," in *Proceedings of the Second Gondwana Symposium*, ed. S. H. Haughton (New Delhi: Council for Scientific and Industrial Research), 309–312.

Kitching, J. W. (1977). *The Distribution of the Karoo vertebrate fauna: Memoir of the Bernard Price Institute for Palaeontological Research*. Johannesburg: University of the Witwatersrand, 1–131.

Li, J., Gastaldo, R. A., Neveling, J., and Geissman, J. W. (2017). Siltstones across the *Daptocephalus* (*Dicynodon*) and *Lystrosaurus* assemblage zones, Karoo Basin, South Africa, show no evidence for aridification. *J. Sediment. Res.* 87, 653–671. doi: 10.2110/jsr.2017.35

Li, M., Ogg, J., Zhang, Y., Huang, C., Hinnov, L., Chen, Z.-Q., et al. (2016). Astronomical tuning of the end-permian extinction and the early triassic Epoch of South China and Germany. *Earth Planet. Sci. Lett.* 441, 10–25. doi: 10.1016/j.epsl.2016.02.017

Lindeque, A., De Wit, M. J., Ryberg, T., Weber, M., and Chevalier, L. (2011). Deep crustal profile across the southern Karoo Basin and Beattie Magnetic Anomaly, South Africa: an integrated interpretation with tectonic implications. *S. Afr. J. Geol.* 114, 265–292. doi: 10.2113/gssajg.114.3-4.265

Lucas, S. G. (2017). Permian tetrapod extinction events. *Earth Sci. Rev.* 170, 31–60. doi: 10.1016/j.earscirev.2017.04.008

Lucas, S. G. (2018). "Permian tetrapod biochronology, correlation and evolutionary events," in *The Permian Timescale*, eds S. G. Lucas and S. Z. Shen (London: Geological Society).

MacLeod, K. G., Quinton, P. C., and Bassett, D. J. (2017). Warming and increased aridity during the earliest Triassic in the Karoo Basin. *S. Afr. Geol.* 45, 483–486. doi: 10.1130/g38957.1

MacLeod, K. G., Smith, R. M. H., Koch, P. L., and Ward, P. D. (2000). Timing of mammal-like reptile extinctions across the Permian-Triassic boundary in South Africa. *Geology* 28, 227–230. doi: 10.1130/0091-7613(2000)028<0227:tomlre>2.3.co;2

McCrea, J. M. (1950). On the isotopic chemistry of carbonates and a paleotemperature scale. *J. Chem. Phys.* 18, 849–857. doi: 10.1063/1.1747785

Neveling, J., Gastaldo, R. A., and Geissman, J. W. (2016a). "The Permo–Triassic Boundary in the Karoo Basin," in *Proceedings of the 35th International Geological Congress Pre-Meeting Field Trip Guide P-3, Council for Geoscience*, Pretoria.

Neveling, J., Gastaldo, R. A., Kamo, S. L., Geissman, J. W., Looy, C., et al. (2016b). "A review of stratigraphic, geochemical, and paleontologic correlation data of the terrestrial end-Permian record in South Africa," in *The Origin and Evolution of the Cape Mountains and Karoo Basin*, eds M. J. de Wit and B. Linol (Cham: Springer Publishing), 151–157. doi: 10.1007/978-3-319-40859-0_15

Neymark, L. A., Paces, J. B., Marshall, B. D., Peterman, Z. E., and Whelan, J. F. (2005). Geochemical and C, O, Sr, and U-series isotopic evidence for the meteoric origin of calcrete at Solitario Wash, Crater Flat, Nevada, USA. *Environ. Geol.* 48, 450–465. doi: 10.1007/s00254-005-1260-z

Osborne, C. P., and Beerling, D. J. (2006). Nature's green revolution: the remarkable evolutionary rise of C4 plants. *Philos. Trans. R. Soc. Lond. B Biol. Sci.* 361, 173–194. doi: 10.1098/rstb.2005.1737

Pace, D. W., Gastaldo, R. A., and Neveling, J. (2009). Early Triassic aggradational and degradational landscapes of the Karoo basin and evidence for climate oscillation following the P-Tr Event. *J. Sediment. Res.* 79, 316–331. doi: 10.2110/jsr.2009.036

Retallack, G. J., Metzger, C. A., Greaver, T., Jahren, A. H., Smith, R. M. H., and Sheldon, N. D. (2006). Middle-Late Permian mass extinction on land. *Geol. Soc. Am. Bull.* 118, 1398–1411. doi: 10.1130/B26011.1

Retallack, G. J., Smith, R. M., and Ward, P. D. (2003). Vertebrate extinction across the Permian–Triassic boundary in the Karoo Basin, South Africa. *Geol. Soc. Am. Bull.* 115, 1133–1152. doi: 10.1130/b25215.1

Rey, K., Amiot, R., Fourél, F., Rigaudier, T., Abdala, F., Day, M. O., et al. (2016). Global climate perturbations during the Permo-Triassic mass extinctions recorded by continental tetrapods from South Africa. *Gondwana Res.* 37, 384–396. doi: 10.1016/j.gr.2015.09.008

Romanek, C. S., Grossman, E. L., and Morse, J. W. (1992). Carbon isotopic fractionation in synthetic aragonite and calcite: effects of temperature and precipitation rate. *Geochim. Cosmochim. Acta* 56, 419–430. doi: 10.1016/0016-7037(92)90142-6

Rowe, P. J., and Maher, B. A. (2000). 'Cold' stage formation of calcrete nodules in the Chinese Loess Plateau: evidence from U-series dating and stable isotope analysis. *Palaeogeogr. Palaeoclimatol. Palaeoecol.* 157, 109–125. doi: 10.1016/s0031-0182(99)00157-1

Royer, D. L. (1999). Depth to pedogenic carbonate horizon as a paleoprecipitation indicator? *Geology* 27, 1123–1126. doi: 10.1130/0091-7613(1999)027<1123:dtpcha>2.3.co;2

Rubidge, B. S. (ed.) (1995). Biostratigraphy of the Beaufort Group (Karoo Supergroup). *Geol. Surv. S. Afr. Biostratigraphic Ser.* 1, 1–46.

Rubidge, B. S., Erwin, D. H., Ramezani, J., Bowring, S. A., and de Klerk, W. J. (2013). High-precision temporal calibration of Late Permian vertebrate biostratigraphy: U-Pb zircon constraints from the Karoo Supergroup, South Africa. *Geology* 41, 363–366. doi: 10.1130/g33622.1

Schmid, S., Worden, R. H., and Fisher, Q. J. (2006). Variations of stable isotopes with depth in regolith calcite cements in the Broken Hill region, Australia: palaeoclimate evolution signal? *J. Geochem. Explorat.* 89, 355–358. doi: 10.1016/j.gexplo.2005.11.063

Sheldon, N. D., and Tabor, N. J. (2009). Quantitative paleoenvironmental and paleoclimatic reconstruction using paleosols. *Earth Sci. Rev.* 95, 1–52. doi: 10.1016/j.earscirev.2009.03.004

Sikes, N. E., and Ashley, G. M. (2007). Stable isotopes of pedogenic carbonates as indicators of paleoecology in the Plio-Pleistocene (upper Bed I), western margin of the Olduvai Basin, Tanzania. *J. Hum. Evol.* 53, 574–594. doi: 10.1016/j.jhevol.2006.12.008

Slate, J. L., Smith, G. A., Wang, Y., and Cerling, T. E. (1996). Carbonate-paleosol genesis in the Plio-Pleistocene St. David Formation, southeastern Arizona. *J. Sediment. Res.* 66, 85–94.

Smith, R. H. M., and Botha-Brink, J. (2014). Anatomy of a mass extinction: sedimentological and taphonomic evidence for drought-induced die-offs at the Permo-Triassic boundary in the main Karoo Basin, South Africa. *Palaeogeogr. Palaeoclimatol. Palaeoecol.* 396, 99–118. doi: 10.1016/j.palaeo.2014.01.002

Smith, R. M. H. (1995). Changing fluvial environments across the Permian-Triassic boundary in the Karoo Basin, South Africa, and possible causes of the extinctions. *Palaeogeogr. Palaeoclimatol. Palaeoecol.* 117, 81–104. doi: 10.1016/0031-0182(94)00119-s

Smith, R. M. H., Rubidge, B. S., Day, M. O., and Botha, J. (2020). Introduction to the tetrapod biozonation of the Karoo Supergroup, South African. *J. Sci.* 123, 131–140. doi: 10.25131/sajg.123.0009

Smith, R. M. H., and Ward, P. D. (2001). Pattern of vertebrate extinctions across an event at the Permian-Triassic boundary in the Karoo Basin of South Africa. *Geology* 29, 1147–1150. doi: 10.1130/0091-76132001029

South African Committee for Stratigraphy [SACS] (1980). *Stratigraphy of South Africa. Part 1: Africa, South West Africa/Namibia, and the republics of Bophuthatswana, Transkei and Venda*. Pretoria: Geological Survey of South Africa, 535–548.

Tabor, N. J., Montañez, I. P., and Southard, R. J. (2002). Paleoenvironmental reconstruction from chemical and isotopic compositions of Permo-Pennsylvanian pedogenic minerals. *Geochim. Cosmochim. Acta* 66, 3093–3107. doi: 10.1016/S0016-7037(02)00879-7

Tabor, N. J., Montañez, I. P., Steiner, M. B., and Schwindt, D. (2007). 13C values of carbonate nodules across the Permian-Triassic boundary in the Karoo Supergroup (South Africa) reflect a stinking sulfurous swamp, not atmospheric CO2. *Palaeogeogr. Palaeoclimatol. Palaeoecol.* 252, 370–381. doi: 10.1016/j.palaeo .2006 .11 .047

Viglietti, P. A. (2020). Biostratigraphy of the *Daptocephalus* assemblage zone (Beaufort Group, Karoo Supergroup), South Africa. *S. Afr. J. Geol.* 123, 191–206. doi: 10.25131/sajg.123.0014

Viglietti, P. A., Rubidge, B. S., and Smith, R. M. H. (2017). New late permian tectonic model for South Africa's Karoo Basin: foreland tectonics and climate change before the end-Permian crisis. *Sci. Rep.* 7:10861.

Viglietti, P. A., Smith, R. M. H., Angielczyk, K. D., Kammerer, C. F., Fröbisch, J., and Rubidge, B. S. (2016). The *Daptocephalus* assemblage zone (Lopingian), South Africa: a proposed biostratigraphy based on a new compilation of stratigraphic ranges. *J. Afr. Earth Sci.* 113, 153–164. doi: 10.1016/j.jafrearsci.2015.10.011

Viglietti, P. A., Smith, R. M. H., and Compton, J. S. (2013). Origin and palaeoenvironmental significance of *Lystrosaurus* bonebeds in the earliest Triassic Karoo Basin, South Africa. *Palaeogeogr. Palaeoclimatol. Palaeoecol.* 392, 9–21. doi: 10.1016/j.palaeo.2013.08.015

Ward, P. D., Botha, J., Buick, R., DeKock, M. O., Erwin, D. H., Garrison, G., et al. (2005). Abrupt and gradual extinction among Late Permian land vertebrates in the Karoo Basin, South Africa. *Science* 307, 709–714. doi: 10.1126/science.1107068

Ward, P. D., Montgomery, D. R., and Smith, R. H. M. (2000). Altered river morphology in South Africa related to the Permian-Triassic extinction. *Science* 289, 1740–1743. doi: 10.1126/science.289.5485.1740

Wu, H., Zhang, S., Hinnov, L. A., Jiang, G., Feng, Q., Li, H., et al. (2013). Time-calibrated Milankovitch cycles for the late Permian. *Nat. Commun.* 4:2452. doi: 10.1038/ncomms3452

Conflict of Interest: The authors declare that the research was conducted in the absence of any commercial or financial relationships that could be construed as a potential conflict of interest.